

## Report



**Cite this article:** Vittadello ST, McCue SW, Gunasingh G, Haass NK, Simpson MJ. 2019 Mathematical models incorporating a multi-stage cell cycle replicate normally-hidden inherent synchronization in cell proliferation. *J. R. Soc. Interface* **16**: 20190382. <http://dx.doi.org/10.1098/rsif.2019.0382>

Received: 5 June 2019

Accepted: 26 July 2019

### Subject Category:

Life Sciences–Mathematics interface

### Subject Areas:

systems biology, biomathematics, computational biology

### Keywords:

cell proliferation, synchronization, reproducibility, cell cycle, fluorescent ubiquitination-based cell cycle indicator, mathematical model

### Author for correspondence:

Matthew J. Simpson  
e-mail: matthew.simpson@qut.edu.au

<sup>†</sup>These authors contributed equally to the study.

Electronic supplementary material is available online at <https://dx.doi.org/10.6084/m9.figshare.c.4608440>.

# Mathematical models incorporating a multi-stage cell cycle replicate normally-hidden inherent synchronization in cell proliferation

Sean T. Vittadello<sup>1</sup>, Scott W. McCue<sup>1</sup>, Gency Gunasingh<sup>2</sup>, Nikolas K. Haass<sup>2,†</sup> and Matthew J. Simpson<sup>1,†</sup>

<sup>1</sup>School of Mathematical Sciences, Queensland University of Technology, Brisbane, Queensland 4001, Australia

<sup>2</sup>The University of Queensland, The University of Queensland Diamantina Institute, Translational Research Institute, Woolloongabba, Brisbane, Queensland 4102, Australia

ID STV, 0000-0002-4476-6732; NKH, 0000-0002-3928-5360; MJS, 0000-0001-6254-313X

We present a suite of experimental data showing that cell proliferation assays, prepared using standard methods thought to produce asynchronous cell populations, persistently exhibit inherent synchronization. Our experiments use fluorescent cell cycle indicators to reveal the normally hidden cell synchronization, by highlighting oscillatory subpopulations within the total cell population. These oscillatory subpopulations would never be observed without these cell cycle indicators. On the other hand, our experimental data show that the total cell population appears to grow exponentially, as in an asynchronous population. We reconcile these seemingly inconsistent observations by employing a multi-stage mathematical model of cell proliferation that can replicate the oscillatory subpopulations. Our study has important implications for understanding and improving experimental reproducibility. In particular, inherent synchronization may affect the experimental reproducibility of studies aiming to investigate cell cycle-dependent mechanisms, including changes in migration and drug response.

## 1. Introduction

Cell proliferation is essential for a range of normal and pathological processes. Many different mathematical models of proliferation have been proposed [1–7]. It is often assumed that cells proliferate exponentially

$$\frac{dM(t)}{dt} = \lambda M(t), \quad M(t) = M(0) e^{\lambda t}, \quad (1.1)$$

where  $M(t)$  is the number of cells at time  $t$  and  $\lambda > 0$  is the proliferation rate.

The eukaryotic cell cycle consists of four phases in sequence, namely gap 1 (G1), synthesis (S), gap 2 (G2) and mitosis (M) (figure 1a). A key assumption implicit in equation (1.1) is that the cell population is asynchronous, meaning that the cells are distributed randomly among the cell cycle phases (figure 1b), yielding a constant *per capita* growth rate,  $(1/M(t)) dM(t)/dt = \lambda$ . By contrast, a population of cells is synchronous if the cells are in the same cell cycle phase (figure 1c), or partially synchronous if only a subpopulation of cells is synchronous (figure 1d). In this case, the synchronous cells divide as a cohort in discrete stages, producing a variable *per capita* growth rate. In addition to the implicit assumption of asynchronicity, classical exponential growth models and generalizations thereof [8] do not account for subpopulations, and predict monotonic population growth.

Here we provide new experimental data from two-dimensional cell proliferation assays in which the cell growth appears exponential as in equation (1.1). Unexpectedly, however, we observe oscillatory subpopulations arising from a phenomenon we refer to as *inherent synchronization*. We reveal the normally hidden inherent synchronization by identifying subpopulations based on cell

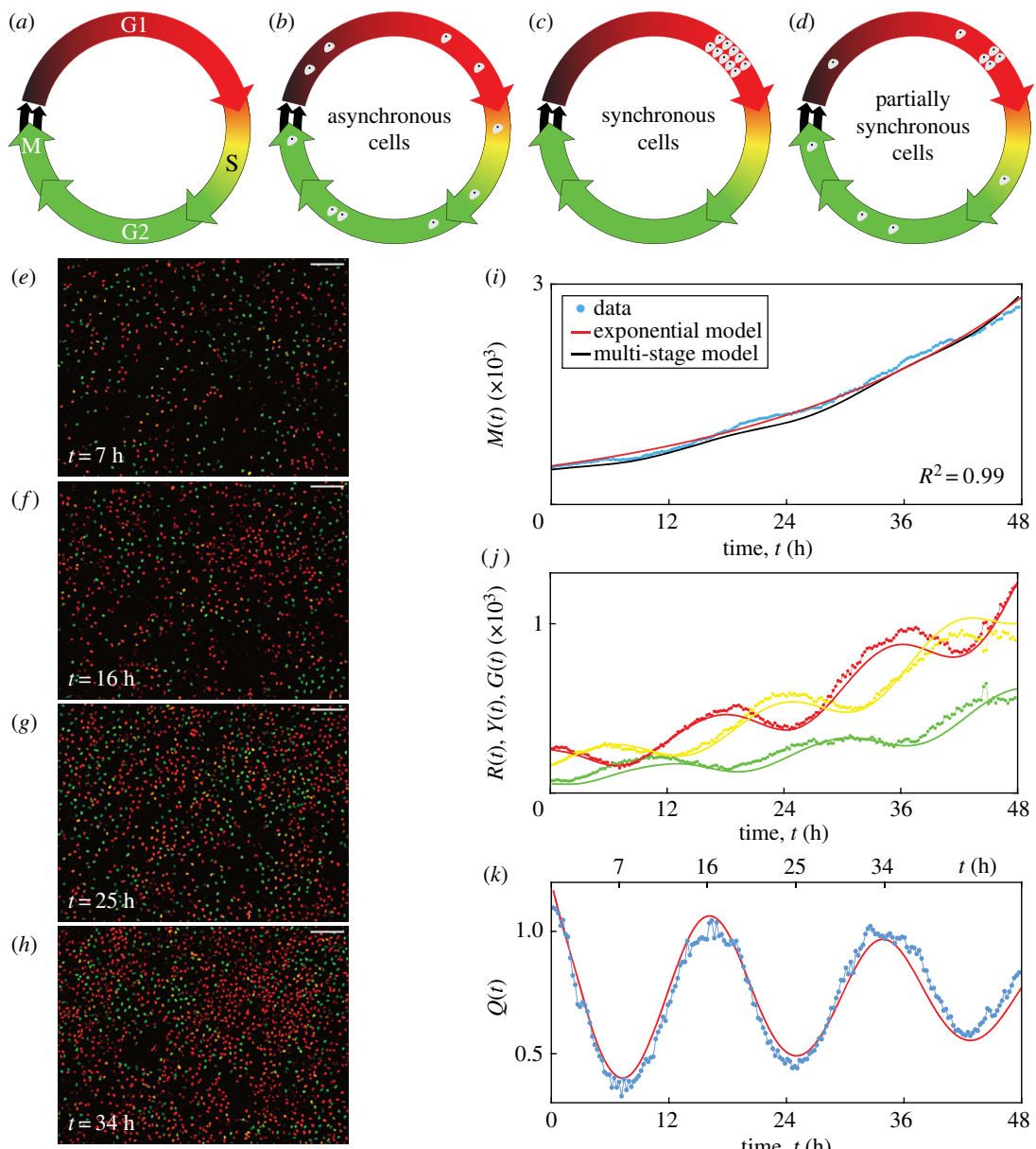


**Figure 1.** C8161 experimental data and multi-stage model solution. (a) The cell cycle, indicating the colour of FUCCI in each phase. (b–d) Asynchronous, synchronous and partially synchronous cells. (e–h) Images of a proliferation assay with FUCCI-C8161 cells. Scale bar, 200 µm. (i)  $M(t)$ . Linear regression of  $\ln M(t)$  versus  $t$  gives  $R^2 = 0.99$ . (j)  $R(t)$ ,  $Y(t)$  and  $G(t)$ . (k)  $Q(t)$ . Experimental data are shown as discs and the model solutions as curves. (Online version in colour.)

cycle phase, employing fluorescent ubiquitination-based cell cycle indicator (FUCCI) [9]. FUCCI enables visualization of the cell cycle of individual live cells via two sensors: when the cell is in G1 the nucleus fluoresces red, and when the cell is in S/G2/M the nucleus fluoresces green. During the G1/S transition, called early S (eS), both sensors fluoresce and the nucleus appears yellow (figure 1a). We explain these seemingly inconsistent observations by applying a multi-stage mathematical model for cell proliferation.

Previous studies of cell synchronization using FUCCI induce the synchronization using methods including serum starvation, cell cycle-inhibiting drugs, environmental pH or contact inhibition [10–15]. Our assays are prepared using a standard method [10] normally thought to produce asynchronous populations, and we take utmost care to ensure that there is no induced synchronization in our cell cultures due to serum starvation, low pH or contact inhibition (electronic supplementary material, S1). Over three cell lines and four independent experiments, however, we consistently observe inherent synchronization.

Neglecting synchronous subpopulations can have important implications for experiment reproducibility. For example, the accurate experimental evaluation of cell cycle-inhibiting drugs is highly dependent on the cell cycle distribution of the cell population [10,16]. In a partially synchronous population, the drug may have a delayed or advanced effect compared with an asynchronous population, depending on the cell cycle position of the synchronous cells. Generally, the presence of synchronization may affect the reproducibility of experiments that investigate cell cycle-dependent mechanisms, such as changes in migration and drug response. Revealing any synchronization with quantitative techniques like FUCCI will lead to a better understanding of these mechanisms.

## 2. Results

### 2.1. Experimental data

Our experimental data are time-series images from two-dimensional proliferation assays using three melanoma cell

lines, C8161, WM983C and 1205Lu [15,17,18], which have mean cell cycle durations of approximately 18, 27 and 36 h, respectively [15]. Four independent experiments are performed for each cell line. Live-cell images are acquired at 15 min intervals over 48 h.

Images from one position in a single well of a FUCCI-C8161 proliferation assay at 7, 16, 25 and 34 h show red, yellow or green nuclei corresponding to the phases G1, eS or S/G2/M (figure 1e–h). We quantify the population growth by counting the total number of cells in each image (electronic supplementary material, S1) to give  $M(t)$  at time  $t$  (figure 1i). The total number of cells appears to grow exponentially over 48 h, supported by the best fit of equation (1.1) (electronic supplementary material, S1) since we have  $R^2 = 0.99$  from the linear regression of  $\ln M(t)$  versus  $t$ . The temporal variations in the numbers of cells in the subpopulations  $R(t)$ ,  $Y(t)$  and  $G(t)$  with red, yellow or green nuclei (figure 1j), respectively, where  $M(t) = R(t) + Y(t) + G(t)$ , are oscillatory. In an asynchronous population, the subpopulations would exhibit monotone growth. The oscillations we observe, however, reveal that the cells are partially synchronous.

To explore the inherent synchronization further, we group cells in eS and S/G2/M together, since eS is part of S, and consider the ratio  $Q(t) = R(t)/(Y(t) + G(t))$  (figure 1k). Synchronization is clearly evident in the oscillatory nature of  $Q(t)$ . Note that the troughs at 7 and 25 h and the peaks at 16 and 34 h are separated by 18 h, which is the approximate cell cycle time for C8161. We can visualize the oscillations in these two subpopulations (figure 1e–h), where the ratio of the number of red cells to the number of yellow and green cells is lower at 7 and 25 h and higher at 16 and 34 h. Equation (1.1) and related generalizations [8] cannot account for the oscillations in these subpopulations. Similar observations are made for further examples of this cell line, and the two additional cell lines (electronic supplementary material, S1). We quantitatively confirm the presence of oscillations in  $Q(t)$ , arising from inherent synchronization, for all 90 datasets by calculating the discrete Fourier transform of the  $Q(t)$  signal, and identifying the dominant frequencies (electronic supplementary material, S1). These results confirm that all 90 experimental replicates display oscillatory subpopulations that are inconsistent with traditional exponential and logistic growth models.

## 2.2. Multi-stage mathematical model

We employ a multi-stage model of cell proliferation [19] which can describe synchronous populations. The model assumes that the cell cycle durations follow a hypoexponential distribution, which consists of a series of independent exponential distributions with different rates. To apply this model, we partition the cell cycle into  $k$  stages,  $P_i$  for  $i = 1, \dots, k$ , where the duration of each  $P_i$  is exponentially distributed with mean  $\mu_i$ . If  $\mathcal{T}$  is the mean cell cycle time then  $\sum_{i=1}^k \mu_i = \mathcal{T}$ . The stages  $P_i$  do not necessarily correspond to phases of the cell cycle, but instead are a mathematical device which allows control over the variance of cell cycle phase durations in the multi-stage model, whereby more stages correspond to less variance in the phase durations for a cell population. If we let the transition rates be  $\lambda_i = 1/\mu_i$  and consider the partitioned cell cycle  $P_1 \xrightarrow{\lambda_1} P_2 \xrightarrow{\lambda_2} \dots \xrightarrow{\lambda_{k-1}} P_k \xrightarrow{\lambda_k} 2P_1$ , we arrive at a system of differential equations describing the mean population  $M_i(t)$  in each

stage [19],

$$\frac{dM_i(t)}{dt} = \begin{cases} 2\lambda_k M_k(t) - \lambda_1 M_1(t), & \text{for } i = 1, \\ \lambda_{i-1} M_{i-1}(t) - \lambda_i M_i(t), & \text{for } i = 2, \dots, k. \end{cases} \quad (2.1)$$

Note that  $M(t) = \sum_{i=1}^k M_i(t)$ . If  $k = 1$ , equation (2.1) simplifies to equation (1.1). Within the 48 h duration of our experiments, none of the cell lines exhibits contact inhibition of proliferation, consistent with the typical loss of contact inhibition in cancer cells [20]. Consequently, a carrying capacity is not incorporated into the model.

We solve equation (2.1) numerically with the forward Euler method, and estimate the parameters by fitting the solution to our experimental data (electronic supplementary material, S1). Using 18 stages for each of the three cell cycle phases described by FUCCI, giving  $k = 54$ , we obtain  $M(t)$  (figure 1i),  $R(t)$ ,  $Y(t)$ ,  $G(t)$  (figure 1j) and  $Q(t)$  (figure 1k), which all correspond well with the experimental data. In particular, the multi-stage model replicates the oscillations in  $R(t)$ ,  $Y(t)$ ,  $G(t)$  and  $Q(t)$ , a feature that is not possible with traditional exponential models. While the multi-stage model can replicate the oscillatory subpopulations, the model is unable to predict all features of the inherent synchronization in a cell proliferation experiment due to variable initial conditions, as the inherent synchronization is a stochastic phenomenon which likely arises from cell division and intercellular interactions. The model can, however, be used to predict general features of the inherent synchronization of each cell line.

## 3. Conclusion

Our new experimental data demonstrate that cell populations may appear to grow exponentially despite subpopulations exhibiting oscillatory growth arising from normally hidden inherent synchronization. We use standard experimental methods thought to produce asynchronous populations; however, all of our proliferation assays exhibit inherent synchronization. We use FUCCI to track cell cycle progression, which is necessary to confirm cell synchronization. As the standard exponential growth model cannot account for subpopulations with oscillating growth, we use a multi-stage mathematical model of cell proliferation to replicate oscillations in population growth. Our results are important because revealing any synchronization will help to better understand cell cycle-dependent mechanisms, such as changes in migration and drug response. Without quantitative techniques like FUCCI to probe the cell cycle, synchronization and its effects on experimental outcomes and reproducibility may remain hidden.

**Data accessibility.** All experimental data are available in the electronic supplementary material documents. All algorithms required to replicate this work are available on GitHub at <https://github.com/ProfMJ Simpson/Vittadello2019>.

**Authors' contributions.** All authors designed the research. S.T.V. performed the research. All authors contributed analytic tools and analysed the data. S.T.V. wrote the manuscript, and all authors approved the final version of the manuscript. N.K.H. and M.J.S. contributed equally.

**Competing interests.** We declare we have no competing interests.

**Funding.** N.K.H. is a Cameron fellow of the Melanoma and Skin Cancer Research Institute and is supported by the NHMRC (APP1084893). M.J.S. is supported by the ARC (DP170100474).

**Acknowledgements.** We thank the editor and four anonymous referees for helpful comments.

## References

1. Sherratt JA, Murray JD. 1990 Models of epidermal wound healing. *Proc. R. Soc. Lond. B* **241**, 29–36. (doi:10.1098/rspb.1990.0061)
2. Swanson KR, Bridge C, Murray JD, Alvord EC. 2003 Virtual and real brain tumors: using mathematical modeling to quantify glioma growth and invasion. *J. Neurol. Sci.* **216**, 1–10. (doi:10.1016/j.jns.2003.06.001)
3. Maini PK, McElwain DLS, Leavesley DL. 2004 Traveling wave model to interpret a wound-healing cell migration assay for human peritoneal mesothelial cells. *Tissue Eng.* **10**, 475–482. (doi:10.1089/107632704323061834)
4. Scott JG, Basanta D, Anderson ARA, Gerlee P. 2013 A mathematical model of tumour self-seeding reveals secondary metastatic deposits as drivers of primary tumour growth. *J. R. Soc. Interface* **10**, 20130011. (doi:10.1098/rsif.2013.0011)
5. Sarapata EA, de Pillis LG. 2014 A comparison and catalog of intrinsic tumor growth models. *Bull. Math. Biol.* **76**, 2010–2024. (doi:10.1007/s11538-014-9986-y)
6. Böttcher MA, Dingli D, Werner B, Traulsen A. 2018 Replicative cellular age distributions in compartmentalized tissues. *J. R. Soc. Interface* **15**, 20180272. (doi:10.1098/rsif.2018.0272)
7. Treloar KK, Simpson MJ, McElwain DLS, Baker RE. 2014 Are *in vitro* estimates of cell diffusivity and cell proliferation rate sensitive to assay geometry?
8. *J. Theor. Biol.* **356**, 71–84. (doi:10.1016/j.jtbi.2014.04.026)
9. Tsouaris A, Wallace J. 2002 Analysis of logistic growth models. *Math. Biosci.* **179**, 21–55. (doi:10.1016/S0025-5564(02)00096-2)
10. Sakaue-Sawano A *et al.* 2008 Visualizing spatiotemporal dynamics of multicellular cell-cycle progression. *Cell* **132**, 487–498. (doi:10.1016/j.cell.2007.12.033)
11. Beaumont KA, Hill DS, Daignault SM, Lui GYL, Sharp DM, Gabrielli B, Weninger W, Haass NK. 2016 Cell cycle phase-specific drug resistance as an escape mechanism of melanoma cells. *J. Invest. Dermatol.* **136**, 1479–1489. (doi:10.1016/j.jid.2016.02.805)
12. Otani K, Naito Y, Sakaguchi Y, Seo Y, Takahashi Y, Kikuta J, Ogawa K, Ishii M. 2016 Cell-cycle-controlled radiation therapy was effective for treating a murine malignant melanoma cell line *in vitro* and *in vivo*. *Sci. Rep.* **6**, 30689. (doi:10.1038/srep30689)
13. Bae H, Go YH, Kwon T, Sung BJ, Cha HJ. 2019 A theoretical model for the cell cycle and drug induced cell cycle arrest of FUCCI systems with cell-to-cell variation during mitosis. *Pharm. Res.* **36**, 57. (doi:10.1007/s11095-019-2570-2)
14. Taylor IW, Hodson PJ. 1984 Cell cycle regulation by environmental pH. *J. Cell. Physiol.* **121**, 517–525. (doi:10.1002/jcp.1041210310)
15. Davis PK, Ho A, Dowdy SF. 2001 Biological methods for cell-cycle synchronization of mammalian cells. *BioTechniques* **30**, 1322–1331. (doi:10.2144/01306rv01)
16. Haass NK, Beaumont KA, Hill DS, Anfosso A, Mrass P, Munoz MA, Kinjyo I, Weninger W. 2014 Real-time cell cycle imaging during melanoma growth, invasion, and drug response. *Pigment. Cell. Melanoma Res.* **27**, 764–776. (doi:10.1111/pcmr.12274)
17. Haass NK, Gabrielli B. 2017 Cell cycle-tailored targeting of metastatic melanoma: challenges and opportunities. *Exp. Dermatol.* **26**, 649–655. (doi:10.1111/exd.13303)
18. Vittadello ST, McCue SW, Gunasingh G, Haass NK, Simpson MJ. 2018 Mathematical models for cell migration with real-time cell cycle dynamics. *Biophys. J.* **114**, 1241–1253. (doi:10.1016/j.bpj.2017.12.041)
19. Simpson MJ, Jin W, Vittadello ST, Tambyah TA, Ryan JM, Gunasingh G, Haass NK, McCue SW. 2018 Stochastic models of cell invasion with fluorescent cell cycle indicators. *Physica A* **510**, 375–386. (doi:10.1016/j.physa.2018.06.128)
20. Hanahan D, Weinberg RA. 2011 Hallmarks of cancer: the next generation. *Cell* **144**, 646–674. (doi:10.1016/j.cell.2011.02.013)

Supporting Information 1 for:

Mathematical models incorporating a multi-stage cell cycle replicate  
normally-hidden inherent synchronisation in cell proliferation

S. T. Vittadello, S. W. McCue, G. Gunasingh, N. K. Haass, M. J. Simpson

# Contents

<b>1 Experimental</b>	<b>3</b>
1.1 Cell culture . . . . .	3
1.2 Proliferation experiments . . . . .	3
1.3 Fluorescent ubiquitination-based cell cycle indicator (FUCCI) . . . . .	4
<b>2 Image processing and analysis</b>	<b>5</b>
2.1 Preprocessing . . . . .	5
2.2 Segmentation . . . . .	5
2.3 Analysis . . . . .	6
<b>3 Parameterisation of the exponential model</b>	<b>8</b>
<b>4 Parameterisation of the multi-stage mathematical model</b>	<b>9</b>
4.1 Method for parameter estimation . . . . .	9
4.2 Specific estimated parameters . . . . .	11
4.2.1 C8161 cell line - Figure 1 . . . . .	12
4.2.2 C8161 cell line, different numbers of stages - Figure S1 . . . . .	13
4.2.3 C8161 cell line - Figure S2 . . . . .	15
4.2.4 C8161 cell line - Figure S3 . . . . .	18
4.2.5 WM983C cell line - Figure S4 . . . . .	20
4.2.6 WM983C cell line - Figure S5 . . . . .	22
4.2.7 WM983C cell line - Figure S6 . . . . .	24
4.2.8 1205Lu cell line - Figure S7 . . . . .	26
4.2.9 1205Lu cell line - Figure S8 . . . . .	29
4.2.10 1205Lu cell line - Figure S9 . . . . .	31

<b>5 All experimental data</b>	<b>33</b>
5.1 C8161 cell line . . . . .	35
5.2 WM983C cell line . . . . .	38
5.3 1205Lu cell line . . . . .	41
<b>References</b>	<b>44</b>

# 1 Experimental

Here we provide details of the experimental methodology that we use for our cell proliferation experiments involving three melanoma cell lines.

## 1.1 Cell culture

The human melanoma cell lines C8161 (kindly provided by Mary Hendrix, Chicago, IL, USA), WM983C and 1205Lu (both kindly provided by Meenhard Herlyn, Philadelphia, PA, USA) were genotypically characterised [1–4], grown as described [5] (using 4% fetal bovine serum instead of 2%), and authenticated by STR fingerprinting (QIMR Berghofer Medical Research Institute, Herston, Australia).

We maintain the cell cultures to prevent any induced synchronisation from cell cycle arrest in G1 phase. In general, such induced synchronisation can occur through various experimental conditions, namely contact inhibition of proliferation at relatively high population densities [6], decreased pH of the growth medium due to the concentration of acidic cell-metabolites such as lactic acid [7], and reduced availability of nutrients such as serum [8]. We prevent induced synchronisation by passaging the cells every three days, and on the day prior to setting up an experiment, to maintain a subconfluent cell density and a fresh growth medium, so that the cell culture conditions are never such that they cause G1 arrest.

## 1.2 Proliferation experiments

Cells are seeded from subconfluent culture flasks onto a 24-well plate at a density of  $10^4$  cells  $\text{cm}^{-2}$ , with 2.5 ml of medium per well, which is 2.5 times the volume of the standard protocol. After incubating the plate for 24 h at 37°C with 5% CO<sub>2</sub>, live-cell images are acquired at 15 minute intervals over 48 h at six different positions of the well. Four independent experiments are performed for each cell line.

Our preliminary experiments used a standard 1 ml of medium in each well, however the cells started to arrest in G1 around 48 hours after seeding, which is likely due to decreased pH of the medium from the lactic acid concentration. We therefore performed a large number of preliminary tests in an attempt to prevent

the cells from arresting in G1 during the experiment, and we found that this is possible by increasing the volume of medium in each well to the reasonable maximum of 2.5 ml, given the volume of each well is 3 ml. The larger volume of medium reduces the rate at which the pH decreases through greater dilution of the acidic-metabolites. The result of the increased volume of medium is that the cells do not begin to arrest in G1 until close to 72 hours following seeding, which provides us with almost 48 hours of imaging using cells that have minimal G1 arrest.

### 1.3 Fluorescent ubiquitination-based cell cycle indicator (FUCCI)

To generate stable melanoma cell lines expressing the FUCCI constructs, mKO2-hCdt1 (30-120) and mAG-hGem (1-110) [9] were subcloned into a replication-defective, self-inactivating lentiviral expression vector system as previously described [5]. The lentivirus was produced by co-transfection of human embryonic kidney 293T cells. High-titer viral solutions for mKO2-hCdt1 (30/120) and mAG-hGem (1/110) were prepared and used for co-transduction into the melanoma cell lines, and subclones were generated by single cell sorting [10–12].

## 2 Image processing and analysis

The microscopy data consist of multi-channel time-series stacks which are processed and analysed automatically with Fiji/ImageJ and MATLAB as described below.

### 2.1 Preprocessing

To maximise the accuracy in identifying particles, which in our case are cell nuclei, we enhance the quality of the microscopy images using ImageJ as follows.

1. Import the time-series stack with the Bio-Formats Importer plugin, splitting the red and green channels.
2. Apply five iterations of Subtract Background with rolling-ball radius of 5 pixels.
3. Apply Enhance Contrast with the Equalize Histogram option selected.
4. Apply the Gaussian Blur filter with sigma = 1.

### 2.2 Segmentation

We now identify the particles in the processed images using ImageJ.

1. Apply Auto-thresholding using the Yen method, selecting the option to ‘calculate the threshold for each image’.
2. The resulting binary images are then refined by applying:
  - (a) Watershed;
  - (b) Fill Holes;
  - (c) Open, with iterations = 10 and count = 5;
  - (d) Watershed.

## 2.3 Analysis

For every image in the segmented binary time-series stacks we count the number of particles in each of the red and green channels using ImageJ. We then use MATLAB to determine which particles are yellow.

1. For each of the red and green channels, apply Analyze Particles in ImageJ with sizes in the range  $5\text{--}\infty$  pixels<sup>2</sup> and the option ‘limit to threshold’ selected. Output the stack position and the centroid of every particle in each channel.
2. We now need to determine which particles are red, yellow or green. A particle is red if it appears in the red channel, and there is no corresponding particle in the green channel. Similarly, a particle is green if it appears in the green channel, and there is no corresponding particle in the red channel. A particle is then yellow if it appears in both the red and green channels. Identifying whether a particle appears in both the red and green channels is complicated by the possible alteration of the shape of the particle during image processing. While we process every image in exactly the same way, the original microscopy images may have different signal-to-noise ratios between the red and green channels. Consequently, there may be a difference in the shape of a particle depending on the channel in which it is viewed, and thereby a difference in the centroid of the particle in each channel. We therefore use MATLAB to determine which particles are red, yellow or green, using the stack position and centroid of each particle, as follows.
  - (a) We first find the yellow particles using the stack position and centroid of each particle, so choose a particle, in turn, from the red channel.
  - (b) Search the green channel for a corresponding particle such that the Euclidean distance between the centroids of the two particles is not greater than 3 pixels, noting that the pixel size in our images is  $1.8150 \mu\text{m}$ . This distance allows for a location error of the centroids of the red and green particles, whereby the centroids may be translated up to one pixel from the original centroid of the yellow particle in the unprocessed images. Placing the original yellow centroid at the centre of a  $3 \times 3$

grid of pixels, the red and green centroids from the processed images may be located at any of the nine pixels in the grid.

- (c) Once all of the yellow particles are found, the red particles are all of the particles in the red channel which are not yellow. Similarly, the green particles are all of the particles in the green channel which are not yellow.

### 3 Parameterisation of the exponential model

To estimate the parameters of the exponential model Equation (1) when fitting the model solution to the experimental data for the total number of cells, we use the `fit` function and `exp1` model [13] in MATLAB. The parameter estimates, with 95% confidence intervals, are:

- **C8161 cell line - Figure 1(i)**

$$M(0) = 524.3 \text{ (515.1, 533.4)} \text{ and } \lambda = 0.03504 \text{ h}^{-1} \text{ (0.03456, 0.03551).}$$

- **C8161 cell line - Figure S2(e)**

$$M(0) = 386.4 \text{ (382.2, 390.5)} \text{ and } \lambda = 0.0316 \text{ h}^{-1} \text{ (0.0313, 0.0319).}$$

- **C8161 cell line - Figure S3(e)**

$$M(0) = 401 \text{ (393.8, 408.2)} \text{ and } \lambda = 0.03573 \text{ h}^{-1} \text{ (0.03525, 0.03622).}$$

- **WM983C cell line - Figure S4(e)**

$$M(0) = 247.7 \text{ (244.3, 251.2)} \text{ and } \lambda = 0.02541 \text{ h}^{-1} \text{ (0.02501, 0.02581).}$$

- **WM983C cell line - Figure S5(e)**

$$M(0) = 366.4 \text{ (362.8, 370)} \text{ and } \lambda = 0.01917 \text{ h}^{-1} \text{ (0.01888, 0.01946).}$$

- **WM983C cell line - Figure S6(e)**

$$M(0) = 158 \text{ (155.4, 160.7)} \text{ and } \lambda = 0.0175 \text{ h}^{-1} \text{ (0.01699, 0.01801).}$$

- **1205Lu cell line - Figure S7(e)**

$$M(0) = 215.9 \text{ (214.1, 217.7)} \text{ and } \lambda = 0.01932 \text{ h}^{-1} \text{ (0.01907, 0.01958).}$$

- **1205Lu cell line - Figure S8(e)**

$$M(0) = 249.1 \text{ (246.5, 251.7)} \text{ and } \lambda = 0.01934 \text{ h}^{-1} \text{ (0.01903, 0.01965).}$$

- **1205Lu cell line - Figure S9(e)**

$$M(0) = 266.6 \text{ (263.6, 269.6)} \text{ and } \lambda = 0.01926 \text{ h}^{-1} \text{ (0.01893, 0.0196).}$$

## 4 Parameterisation of the multi-stage mathematical model

Here we describe our methodology for estimating the parameters of the multi-stage mathematical model, Equation (2), and the procedure we use to calibrate the solution of the model to match the experimental data.

### 4.1 Method for parameter estimation

The multi-stage model requires specification of the number of stages, the transition rates from each stage to the successive stage, and the initial population in each stage. In this work, we aim to achieve the best fit of the model to our data while keeping the number of model parameters with distinct values to a minimum.

We partition the phases G1, eS and S/G2/M into the same number of stages,  $N$ . The mean durations of the phases G1, eS and S/G2/M are denoted by  $L_r$ ,  $L_y$  and  $L_g$ , respectively. The transition rates between successive stages are set equal within each phase to  $N/L_r$  in G1,  $N/L_y$  in eS, and  $N/L_g$  in S/G2/M. For each  $i = 1, \dots, N$  we denote the mean number of cells at time  $t$  in stage  $i$  of G1 as  $R_i(t)$ , of eS as  $Y_i(t)$ , and of S/G2/M as  $G_i(t)$ . Therefore,  $R(t) = \sum_{i=1}^N R_i(t)$ ,  $Y(t) = \sum_{i=1}^N Y_i(t)$ , and  $G(t) = \sum_{i=1}^N G_i(t)$ . The parameters that we need to estimate are the components of the vector

$$\mathbf{x} = [R_1(0) \dots R_N(0) \quad Y_1(0) \dots Y_N(0) \quad G_1(0) \dots G_N(0) \quad L_r \quad L_y \quad L_g]. \quad (\text{S1})$$

The parameters in Equation (S1) are either numbers of cells or phase durations, which are all non-negative, so we require our optimisation algorithm to accept bound constraints. To find estimates for these parameters we use the MATLAB nonlinear least-squares solver `lsqnonlin` [14] with the trust-region-reflective algorithm [15], which allows for bound constraints of the parameters. In the following, a dependent variable has the subscript ‘model’ or ‘data’ to distinguish between model and data values of the variable. With non-negative weights  $w_2, \dots, w_7$ , we define the vector objective function

$$\mathbf{F}(\mathbf{x}) = [\mathbf{f}_1(\mathbf{x}) \quad w_2\mathbf{f}_2(\mathbf{x}) \quad w_3\mathbf{f}_3(\mathbf{x}) \quad w_4\mathbf{f}_4(\mathbf{x}) \quad w_5\mathbf{f}_5(\mathbf{x}) \quad w_6\mathbf{f}_6(\mathbf{x}) \quad w_7\mathbf{f}_7(\mathbf{x})] \quad (\text{S2})$$

as the concatenation of the weight-scaled vectors

$$\mathbf{f}_1(\mathbf{x}) = [ (Q_{\text{model}}(\mathbf{x}) - Q_{\text{data}})(t_1) \quad \dots \quad (Q_{\text{model}}(\mathbf{x}) - Q_{\text{data}})(t_n) ], \quad (\text{S3})$$

$$\mathbf{f}_2(\mathbf{x}) = [ (R_{\text{model}}(\mathbf{x}) - R_{\text{data}})(t_1) \quad \dots \quad (R_{\text{model}}(\mathbf{x}) - R_{\text{data}})(t_n) ], \quad (\text{S4})$$

$$\mathbf{f}_3(\mathbf{x}) = [ (Y_{\text{model}}(\mathbf{x}) - Y_{\text{data}})(t_1) \quad \dots \quad (Y_{\text{model}}(\mathbf{x}) - Y_{\text{data}})(t_n) ], \quad (\text{S5})$$

$$\mathbf{f}_4(\mathbf{x}) = [ (G_{\text{model}}(\mathbf{x}) - G_{\text{data}})(t_1) \quad \dots \quad (G_{\text{model}}(\mathbf{x}) - G_{\text{data}})(t_n) ], \quad (\text{S6})$$

$$\mathbf{f}_5(\mathbf{x}) = [ (G_{\text{model}}(\mathbf{x}) - G_{\text{data}})(t_n) ], \quad (\text{S7})$$

$$\mathbf{f}_6(\mathbf{x}) = [ \mathcal{T} - L_r - L_y - L_g ], \quad (\text{S8})$$

$$\mathbf{f}_7(\mathbf{x}) = [ (M_{\text{model}}(\mathbf{x}) - M_{\text{data}})(t_1) \quad \dots \quad (M_{\text{model}}(\mathbf{x}) - M_{\text{data}})(t_n) ], \quad (\text{S9})$$

where:

1.  $Q_{\text{model}}(\mathbf{x})$  is the ratio of the number of cells in G1 to the number of cells in eS/S/G2/M, from the model solution;
2.  $Q_{\text{data}}$  is the ratio of the number of cells in G1 to the number of cells in eS/S/G2/M, from the data;
3.  $R_{\text{model}}(\mathbf{x})$ ,  $Y_{\text{model}}(\mathbf{x})$  and  $G_{\text{model}}(\mathbf{x})$  are the subpopulations of cells in G1, eS and S/G2/M, respectively, from the model solution;
4.  $R_{\text{data}}$ ,  $Y_{\text{data}}$  and  $G_{\text{data}}$  are the subpopulations of cells in G1, eS and S/G2/M, respectively, from the data;
5.  $M_{\text{model}}(\mathbf{x})$  is the total cell population, from the model solution;
6.  $M_{\text{data}}$  is the total cell population, from the data;
7.  $t_1 < \dots < t_n$  are the data time points over 48 hours;
8.  $\mathcal{T}$  is the cell cycle time.

The vector  $\mathbf{f}_1$  is used to fit the model to the ratio data, and the vectors  $\mathbf{f}_2, \dots, \mathbf{f}_4$  are used to fit the model to the three subpopulations corresponding to G1, eS and S/G2/M. The vector  $\mathbf{f}_5$  fits the model to the S/G2/M subpopulation data at the final time point, and is only required if the cells are starting to arrest in G1 near the end of the experiment due to the decreased pH of the growth medium. The vector  $\mathbf{f}_6$  constrains the estimated phase durations to sum to the expected cell cycle time, and is generally required only when there are an insufficient number of oscillations in  $Q_{\text{data}}(t)$  to bound the estimated cell-phase durations to physically realistic values. The vector  $\mathbf{f}_7$  is used to fit the model to the total population data, and is often not required as a good fit usually follows from fitting to the subpopulations.

Note that the weights in the objective function Equation (S2) are specified prior to optimising the estimates of the parameters in Equation (S1). The weights differ between data sets in order to obtain the best fit of the multi-stage model to each data set.

## 4.2 Specific estimated parameters

Here we provide a summary of the estimated parameters of the multi-stage model Equation (2) corresponding to Figure 1, along with additional data sets from the C8161 (Figures S2–S3), WM983C (Figures S4–S6) and 1205Lu (Figure S7–S9) cell lines. The correspondence between these figures and the data sets in Figures S10–S18 is:

- Figure 1 - First plot in Well 1 of Experiment 2, Figures S10, S11 and S12;
- Figure S2 - Second plot in Well 1 of Experiment 1, Figures S10, S11 and S12;
- Figure S3 - First plot in Well 1 of Experiment 3, Figures S10, S11 and S12;
- Figure S4 - Second plot in Well 1 of Experiment 4, Figures S13, S14 and S15;
- Figure S5 - Fourth plot in Well 1 of Experiment 1, Figures S13, S14 and S15;
- Figure S6 - Third plot in Well 1 of Experiment 2, Figures S13, S14 and S15;

- Figure S7 - First plot in Well 1 of Experiment 4, Figures S16, S17 and S18;
- Figure S8 - Fourth plot in Well 1 Experiment 4, Figures S16, S17 and S18;
- Figure S9 - Fifth plot in Well 2 of Experiment 4, Figures S16, S17 and S18.

#### 4.2.1 C8161 cell line - Figure 1

The experimentally-determined mean cell cycle time for C8161 is approximately  $\mathcal{T} = 18$  h [10]. We partition each cell cycle phase into  $N = 18$  stages, giving a total of  $k = 54$  stages for the complete cell cycle. In each phase we set the first half of the stages, totalling 9 stages, to have equal numbers of cells, and the second half of the stages to have equal numbers of cells. We therefore only require a total of six distinct population parameters.

The vector objective function is  $\mathbf{F}(\mathbf{x}) = [\mathbf{f}_1(\mathbf{x}) \ 10^{-4}\mathbf{f}_2(\mathbf{x}) \ 10^{-4}\mathbf{f}_3(\mathbf{x}) \ 10^{-4}\mathbf{f}_4(\mathbf{x}) \ 10^{-3}\mathbf{f}_5(\mathbf{x})]$ . Starting with the parameters  $R_i(0) = Y_i(0) = G_i(0) = 0.5$  for  $i = 1, \dots, N$ , and  $L_r = L_y = L_g = 6$ , we obtain the parameterisation

$$R_i(0) = \begin{cases} 15.48 & \text{for } i = 1, \dots, 9, \\ 12.93 & \text{for } i = 10, \dots, 18, \end{cases} \quad Y_i(0) = \begin{cases} 12.94 & \text{for } i = 1, \dots, 9, \\ 5.41 & \text{for } i = 10, \dots, 18, \end{cases} \quad L_r = 6.14 \text{ h},$$

$$G_i(0) = \begin{cases} 2.51 & \text{for } i = 1, \dots, 9, \\ 3.48 & \text{for } i = 10, \dots, 18, \end{cases} \quad L_y = 7.43 \text{ h}, \quad L_g = 4.42 \text{ h}. \quad (\text{S10})$$

All parameter estimates given in this document are presented to two decimal places. Note that  $L_r + L_y + L_g = 17.99$  h, in good agreement with the observed cell cycle time of 18 h.

#### 4.2.2 C8161 cell line, different numbers of stages - Figure S1

In Figure S1 we compare solutions of the multi-stage model for  $N = 2, 6, 10$  and  $14$  stages per phase, with the ratio  $Q_{\text{data}}$ . In fitting the model solution we use the same parameters as for Figure 1, except the number

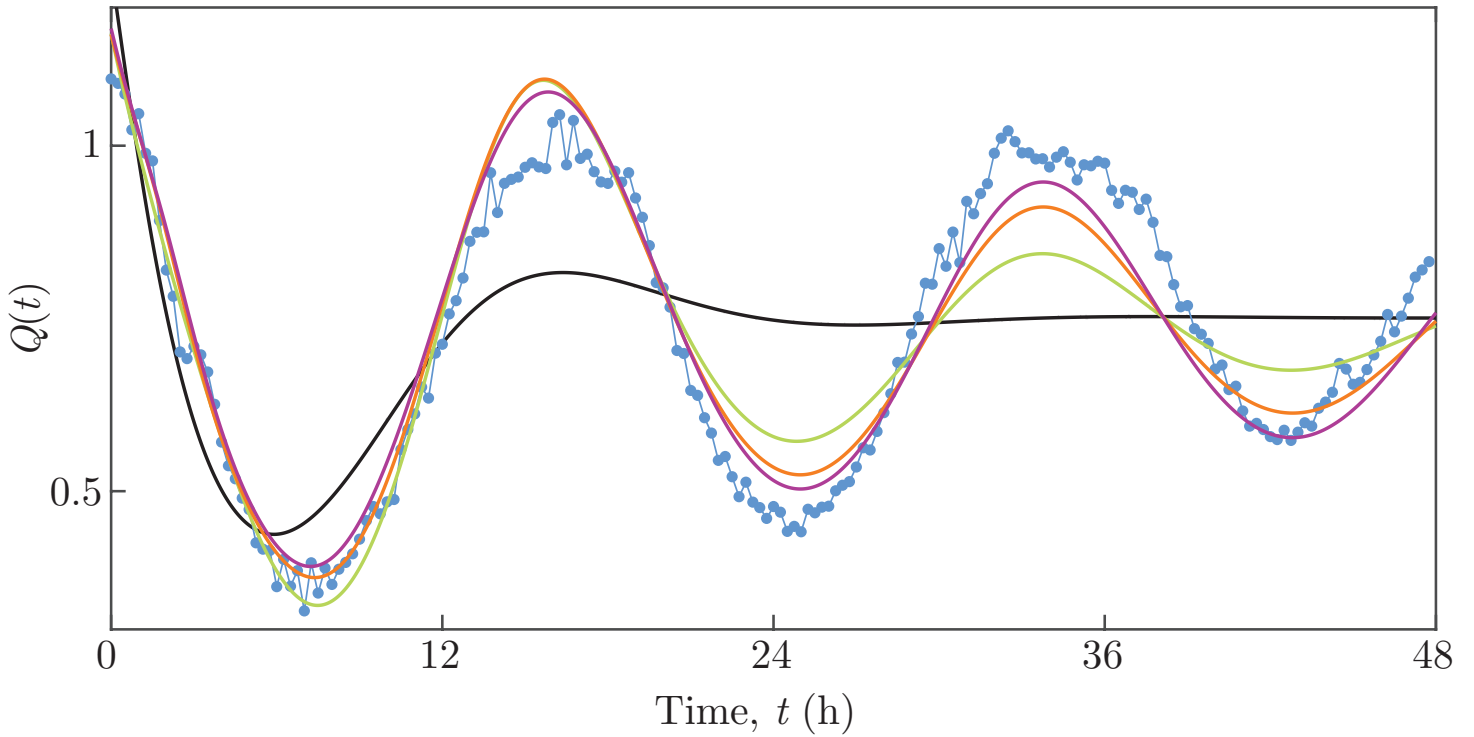


**Figure S1:**  $Q(t)$  for C8161 experimental data and multi-stage model solutions with different numbers of stages. Experimental data are shown as discs and the model solutions as curves. The model solutions with 2, 6, 10 and 14 stages are the black, green, orange and purple curves, respectively.

of stages differ. For each number of stages, in each phase we set the first half of the stages to have equal numbers of cells and the second half of the stages to have equal numbers of cells, so that we therefore only require a total of 6 distinct population parameters. Starting with the parameters  $R_i(0) = Y_i(0) = G_i(0) = 0.5$

for  $i = 1, \dots, N$ , and  $L_r = L_y = L_g = 6$ , the parameterisation for  $N = 14$  is

$$R_i(0) = \begin{cases} 17.89 & \text{for } i = 1, \dots, 9, \\ 18.62 & \text{for } i = 10, \dots, 18, \end{cases} \quad Y_i(0) = \begin{cases} 16.28 & \text{for } i = 1, \dots, 9, \\ 6.77 & \text{for } i = 10, \dots, 18, \end{cases}$$

$$L_r = 6.17 \text{ h}, \quad L_y = 7.27 \text{ h}, \quad L_g = 4.64 \text{ h},$$

$$G_i(0) = \begin{cases} 2.39 & \text{for } i = 1, \dots, 9, \\ 5.78 & \text{for } i = 10, \dots, 18, \end{cases}$$
(S11)

the parameterisation for  $N = 10$  is

$$R_i(0) = \begin{cases} 16.60 & \text{for } i = 1, \dots, 9, \\ 33.58 & \text{for } i = 10, \dots, 18, \end{cases} \quad Y_i(0) = \begin{cases} 20.81 & \text{for } i = 1, \dots, 9, \\ 9.61 & \text{for } i = 10, \dots, 18, \end{cases}$$

$$L_r = 6.22 \text{ h}, \quad L_y = 7.06 \text{ h}, \quad L_g = 4.92 \text{ h},$$

$$G_i(0) = \begin{cases} 0 & \text{for } i = 1, \dots, 9, \\ 12.81 & \text{for } i = 10, \dots, 18, \end{cases}$$
(S12)

the parameterisation for  $N = 6$  is

$$R_i(0) = \begin{cases} 16.42 & \text{for } i = 1, \dots, 9, \\ 66.47 & \text{for } i = 10, \dots, 18, \end{cases} \quad Y_i(0) = \begin{cases} 44.97 & \text{for } i = 1, \dots, 9, \\ 0 & \text{for } i = 10, \dots, 18, \end{cases}$$

$$L_r = 6.28 \text{ h}, \quad L_y = 6.81 \text{ h}, \quad L_g = 5.21 \text{ h},$$

$$G_i(0) = \begin{cases} 0 & \text{for } i = 1, \dots, 9, \\ 26.34 & \text{for } i = 10, \dots, 18, \end{cases}$$
(S13)

and the parameterisation for  $N = 2$  is

$$R_i(0) = \begin{cases} 195.22 & \text{for } i = 1, \dots, 9, \\ 107.41 & \text{for } i = 10, \dots, 18, \end{cases} \quad Y_i(0) = \begin{cases} 241.05 & \text{for } i = 1, \dots, 9, \\ 0 & \text{for } i = 10, \dots, 18, \end{cases}$$

$$L_r = 6.91 \text{ h}, \quad L_y = 7.11 \text{ h}, \quad L_g = 5.79 \text{ h}.$$
(S14)

The corresponding solutions of the multi-stage model are shown in Figure S1.

Considering parameterisations of the model whereby in each phase we set the first half of the stages to have equal numbers of cells and the second half of the stages to have equal numbers of cells, the oscillations decay at a faster rate for a smaller number of stages per phase. A higher number of stages produces a hypoexponential distribution with lower variance, resulting in oscillations which are sustained for longer. Consequently, fewer than 18 stages per phase results in a model solution with a poorer fit.

#### 4.2.3 C8161 cell line - Figure S2

The experimentally-determined mean cell cycle time for C8161 is approximately  $\mathcal{T} = 18$  h [10]. We partition each cell cycle phase into  $N = 40$  stages, giving a total of  $k = 120$  stages for the complete cell cycle. In each phase we set the first half of the stages, totalling 20 stages, to have equal numbers of cells, and the second half of the stages to have equal numbers of cells. We therefore only require a total of six distinct population parameters.

The vector objective function is  $\mathbf{F}(\mathbf{x}) = [\mathbf{f}_1(\mathbf{x}) \ 10^{-3}\mathbf{f}_2(\mathbf{x}) \ 10^{-3}\mathbf{f}_3(\mathbf{x}) \ 10^{-3}\mathbf{f}_4(\mathbf{x})]$ . Trialling different parameters chosen randomly and uniformly from  $(0.1, 1)$  for  $R_i(0)$ ,  $Y_i(0)$  and  $G_i(0)$ , and from  $(4, 8)$  for  $L_r$ ,  $L_y$  and

$L_g$ , we obtain the parameterisation

$$\begin{aligned}
 R_i(0) &= \begin{cases} 2.56 & \text{for } i = 1, \dots, 20, \\ 1.99 & \text{for } i = 21, \dots, 40, \end{cases} & Y_i(0) &= \begin{cases} 5.37 & \text{for } i = 1, \dots, 20, \\ 4.13 & \text{for } i = 21, \dots, 40, \end{cases} \\
 && L_r &= 5.47 \text{ h}, \\
 G_i(0) &= \begin{cases} 0.90 & \text{for } i = 1, \dots, 20, \\ 0.98 & \text{for } i = 21, \dots, 40, \end{cases} & L_y &= 8.67 \text{ h}, \\
 && L_g &= 4.57 \text{ h}.
 \end{aligned} \tag{S15}$$

Note that  $L_r + L_y + L_g = 18.71$  h, in good agreement with the observed cell cycle time of 18 h.

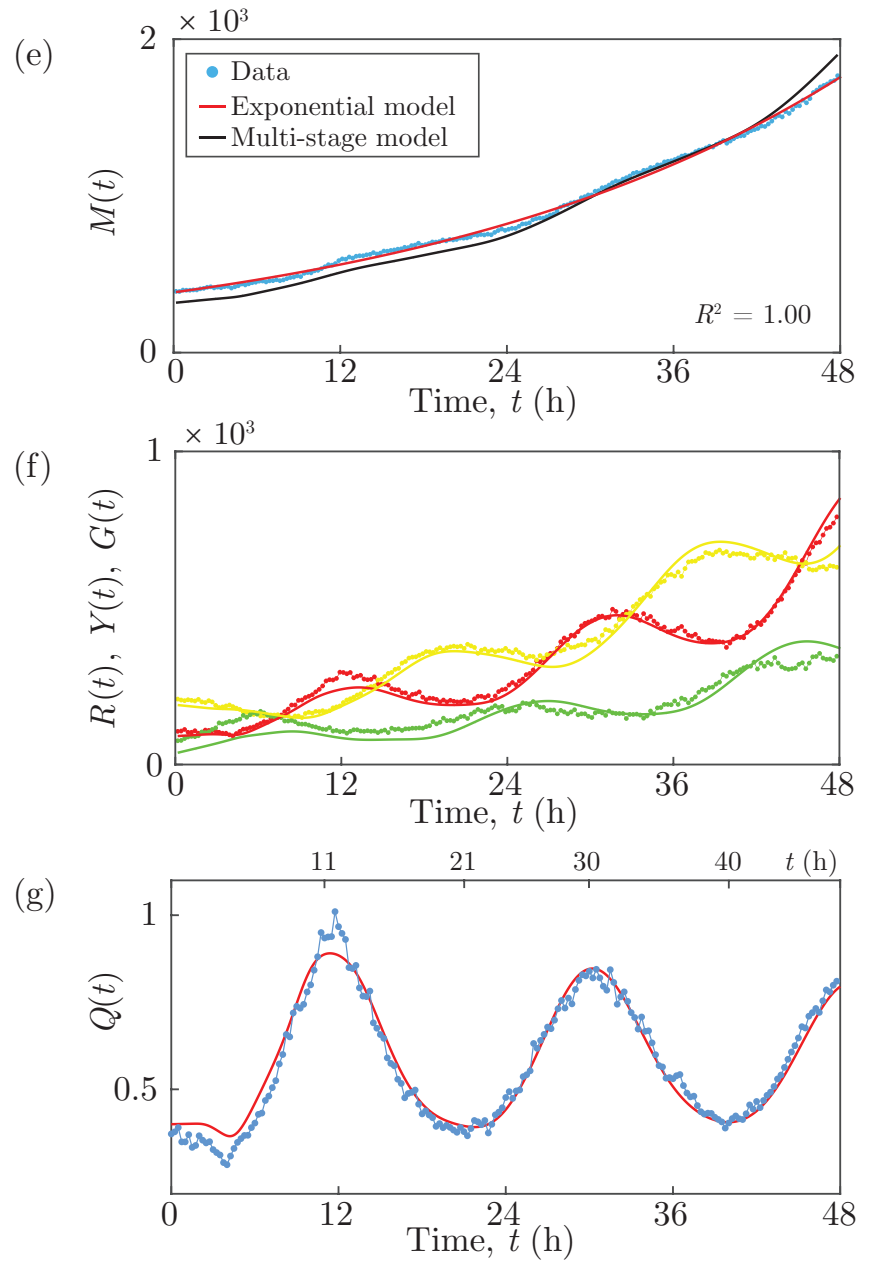
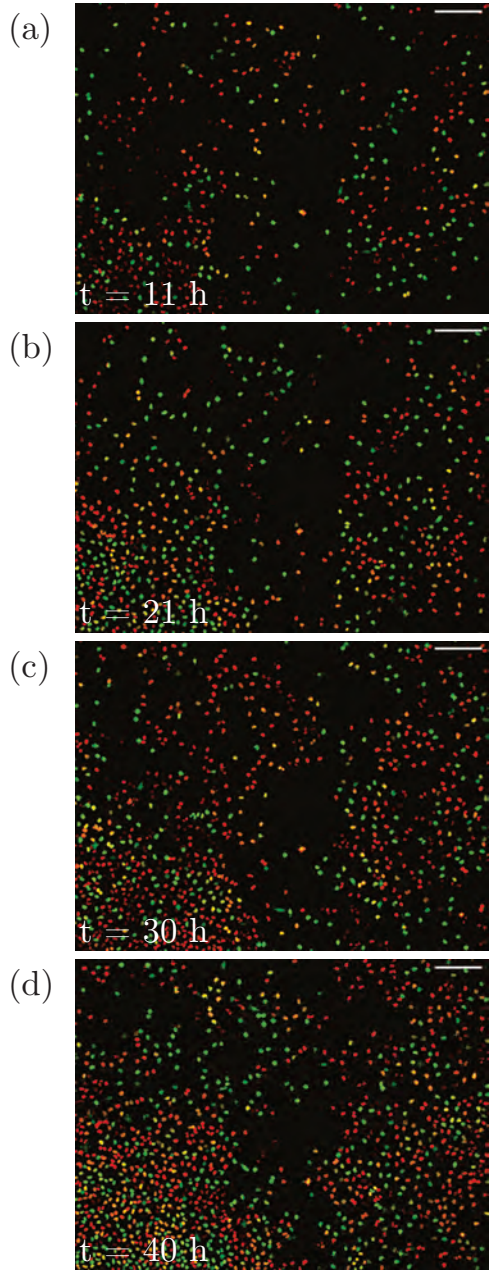


**Figure S2: C8161 experimental data and multi-stage model solution.** (a)–(d) Images of a proliferation assay with FUCCI-C8161 cells. Scale bar 200  $\mu\text{m}$ . (e)  $M(t)$ . Linear regression of  $\ln M(t)$  versus  $t$  provides  $R^2$ . (f)  $R(t)$ ,  $Y(t)$  and  $G(t)$ . (g)  $Q(t)$ . Experimental data are shown as discs and the model solutions as curves.

#### 4.2.4 C8161 cell line - Figure S3

The experimentally-determined mean cell cycle time for C8161 is approximately  $\mathcal{T} = 18$  h [10]. We partition each cell cycle phase into  $N = 40$  stages, giving a total of  $k = 120$  stages for the complete cell cycle. In each phase we set the first half of the stages, totalling 20 stages, to have equal numbers of cells, and the second half of the stages to have equal numbers of cells. We therefore only require a total of six distinct population parameters.

The vector objective function is  $\mathbf{F}(\mathbf{x}) = [\mathbf{f}_1(\mathbf{x}) \ 10^{-4}\mathbf{f}_2(\mathbf{x}) \ 10^{-4}\mathbf{f}_3(\mathbf{x}) \ 10^{-4}\mathbf{f}_4(\mathbf{x}) \ 10^{-3}\mathbf{f}_5(\mathbf{x})]$ . Trialling different parameters chosen randomly and uniformly from  $(0.1, 1)$  for  $R_i(0)$ ,  $Y_i(0)$  and  $G_i(0)$ , and from  $(4, 8)$  for  $L_r$ ,  $L_y$  and  $L_g$ , we obtain the parameterisation

$$R_i(0) = \begin{cases} 3.21 & \text{for } i = 1, \dots, 20, \\ 4.44 & \text{for } i = 21, \dots, 40, \end{cases} \quad Y_i(0) = \begin{cases} 5.03 & \text{for } i = 1, \dots, 20, \\ 2.59 & \text{for } i = 21, \dots, 40, \end{cases} \quad L_r = 6.29 \text{ h},$$

$$G_i(0) = \begin{cases} 1.31 & \text{for } i = 1, \dots, 20, \\ 1.34 & \text{for } i = 21, \dots, 40, \end{cases} \quad L_y = 7.30 \text{ h}, \quad L_g = 4.47 \text{ h}.$$
(S16)

Note that  $L_r + L_y + L_g = 18.06$  h, in good agreement with the observed cell cycle time of 18 h.

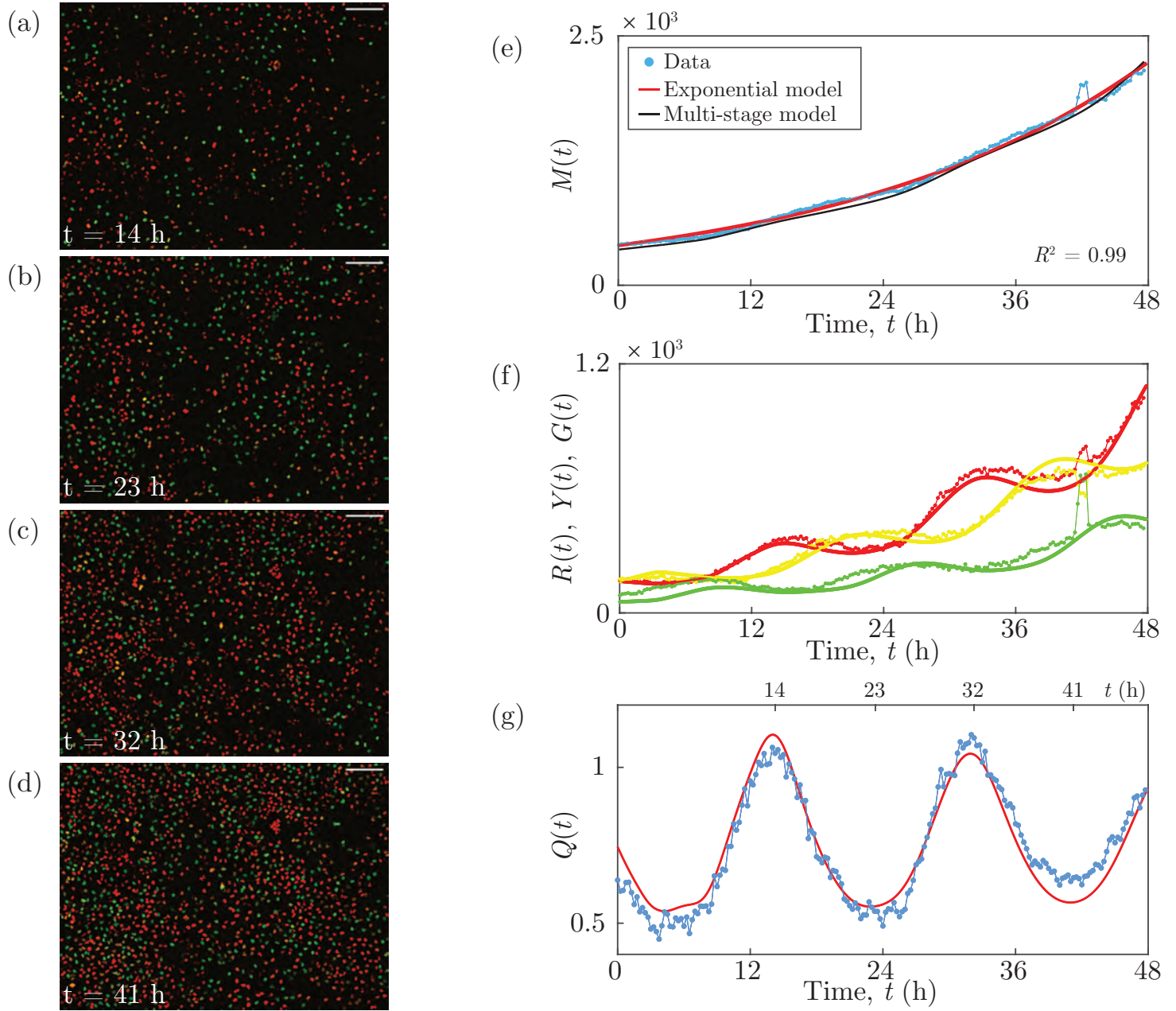


**Figure S3: C8161 experimental data and multi-stage model solution.** (a)–(d) Images of a proliferation assay with FUCCI-C8161 cells. Scale bar 200  $\mu\text{m}$ . (e)  $M(t)$ . Linear regression of  $\ln M(t)$  versus  $t$  provides  $R^2$ . (f)  $R(t)$ ,  $Y(t)$  and  $G(t)$ . (g)  $Q(t)$ . Experimental data are shown as discs and the model solutions as curves.

#### 4.2.5 WM983C cell line - Figure S4

The experimentally-determined mean cell cycle time for WM983C is  $\mathcal{T} = 27$  h [10]. We partition each cell cycle phase into  $N = 10$  stages, giving a total of  $k = 30$  stages for the complete cell cycle. From the start of each phase we set every 2 successive stages to have equal numbers of cells. We therefore only require a total of 15 distinct population parameters.

The vector objective function is  $\mathbf{F}(\mathbf{x}) = [\mathbf{f}_1(\mathbf{x}) \ 10^{-3}\mathbf{f}_2(\mathbf{x}) \ 10^{-3}\mathbf{f}_3(\mathbf{x}) \ 10^{-3}\mathbf{f}_4(\mathbf{x}) \ 10\mathbf{f}_6(\mathbf{x})]$ . Starting with the parameters

$$R_i(0) = \begin{cases} 0 & \text{for } i = 1, 2, \\ 0 & \text{for } i = 3, 4, \\ 29.23 & \text{for } i = 5, 6, \\ 19.66 & \text{for } i = 7, 8, \\ 0 & \text{for } i = 9, 10, \end{cases} \quad Y_i(0) = \begin{cases} 33.02 & \text{for } i = 1, 2, \\ 0 & \text{for } i = 3, 4, \\ 0 & \text{for } i = 5, 6, \\ 0 & \text{for } i = 7, 8, \\ 0 & \text{for } i = 9, 10, \end{cases} \quad (S17)$$

$$G_i(0) = \begin{cases} 11.04 & \text{for } i = 1, 2, \\ 0 & \text{for } i = 3, 4, \\ 4.29 & \text{for } i = 5, 6, \\ 24.41 & \text{for } i = 7, 8, \\ 0 & \text{for } i = 9, 10, \end{cases} \quad L_r = 10.28 \text{ h}, \quad L_y = 3.87 \text{ h}, \quad L_g = 12.85 \text{ h},$$

we obtain the same parameterisation Equation (S17). Note that  $L_r + L_y + L_g = 27.00$  h, in good agreement with the observed cell cycle time of 27 h.

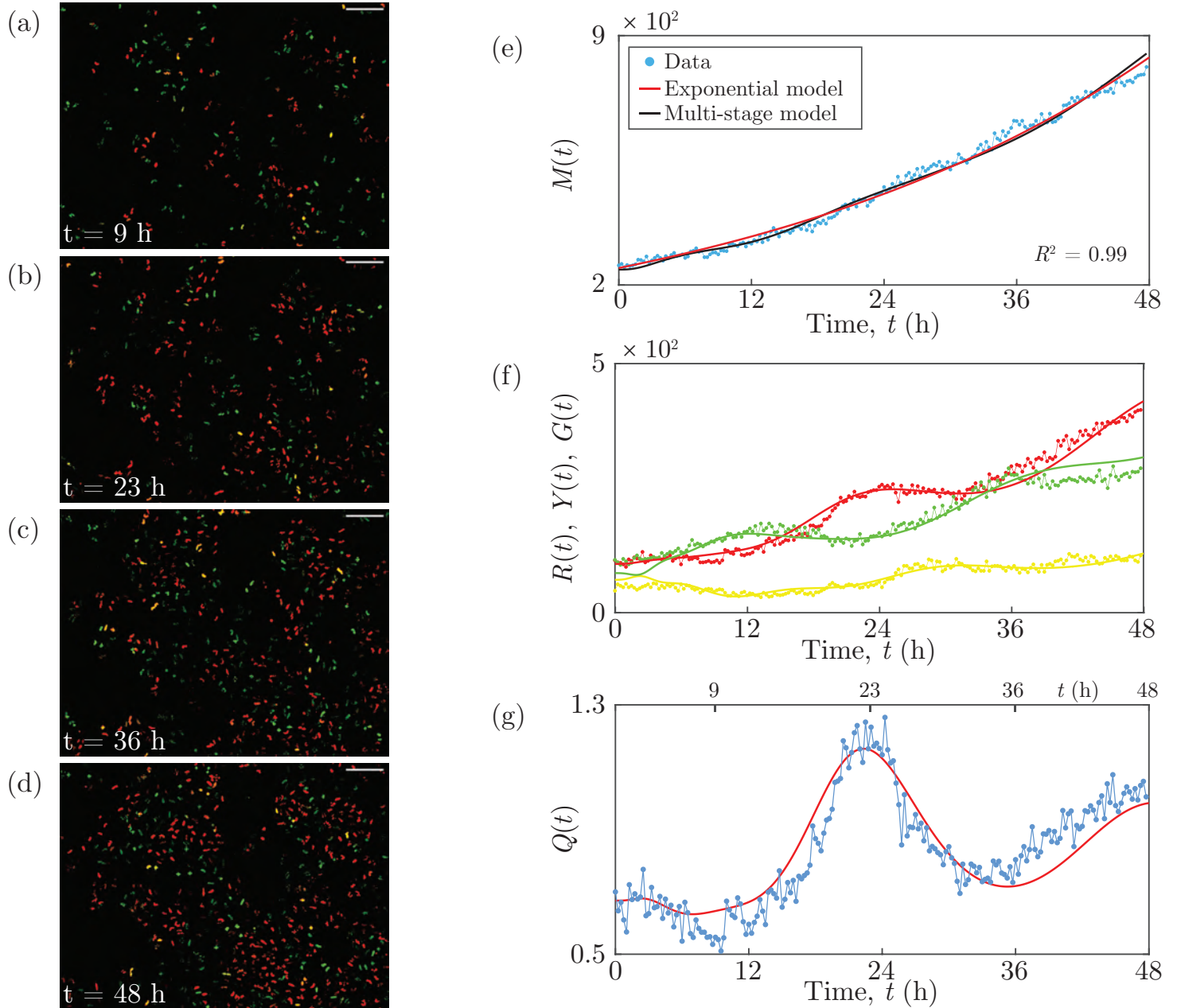


**Figure S4: WM983C experimental data and multi-stage model solution.** (a)–(d) Images of a proliferation assay with FUCCI-WM983C cells. Scale bar 200  $\mu$ m. (e)  $M(t)$ . Linear regression of  $\ln M(t)$  versus  $t$  provides  $R^2$ . (f)  $R(t)$ ,  $Y(t)$  and  $G(t)$ . (g)  $Q(t)$ . Experimental data are shown as discs and the model solutions as curves.

#### 4.2.6 WM983C cell line - Figure S5

The experimentally-determined mean cell cycle time for WM983C is  $\mathcal{T} = 27$  h [10]. We partition each cell cycle phase into  $N = 10$  stages, giving a total of  $k = 30$  stages for the complete cell cycle. From the start of each phase we set every 5 successive stages to have equal numbers of cells. We therefore only require a total of 6 distinct population parameters.

The vector objective function is  $\mathbf{F}(\mathbf{x}) = [\mathbf{f}_1(\mathbf{x}) \ 10^{-3}\mathbf{f}_2(\mathbf{x}) \ 10^{-3}\mathbf{f}_3(\mathbf{x}) \ 10^{-3}\mathbf{f}_4(\mathbf{x}) \ 10^{-3}\mathbf{f}_7(\mathbf{x})]$ . Trialling different parameters chosen randomly and uniformly from  $(0.1, 1)$  for  $R_i(0)$ ,  $Y_i(0)$  and  $G_i(0)$ , and from  $(4, 20)$  for  $L_r$ ,  $L_y$  and  $L_g$ , we obtain the parameterisation

$$R_i(0) = \begin{cases} 12.82 & \text{for } i = 1, \dots, 5, \\ 13.13 & \text{for } i = 6, \dots, 10, \end{cases} \quad Y_i(0) = \begin{cases} 7.86 & \text{for } i = 1, \dots, 5, \\ 8.47 & \text{for } i = 6, \dots, 10, \end{cases} \quad L_r = 9.06 \text{ h},$$

$$G_i(0) = \begin{cases} 18.10 & \text{for } i = 1, \dots, 5, \\ 7.51 & \text{for } i = 6, \dots, 10, \end{cases} \quad L_y = 6.50 \text{ h}, \quad L_g = 15.79 \text{ h}.$$
(S18)

Note that  $L_r + L_y + L_g = 31.35$  h, in good agreement with the observed cell cycle time of 27 h.

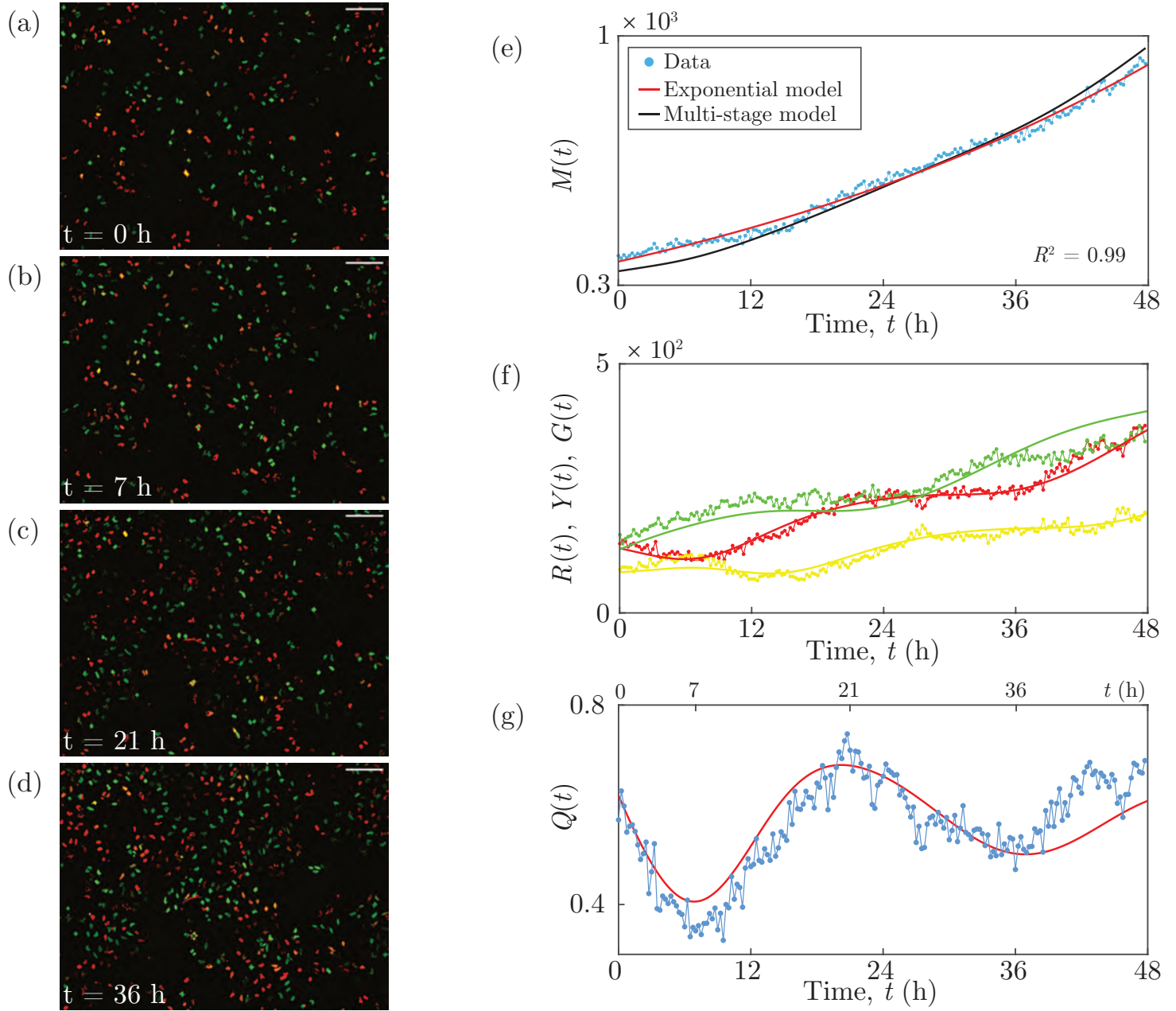


**Figure S5: WM983C experimental data and multi-stage model solution.** (a)–(d) Images of a proliferation assay with FUCCI-WM983C cells. Scale bar 200  $\mu\text{m}$ . (e)  $M(t)$ . Linear regression of  $\ln M(t)$  versus  $t$  provides  $R^2$ . (f)  $R(t)$ ,  $Y(t)$  and  $G(t)$ . (g)  $Q(t)$ . Experimental data are shown as discs and the model solutions as curves.

#### 4.2.7 WM983C cell line - Figure S6

The experimentally-determined mean cell cycle time for WM983C is  $\mathcal{T} = 27$  h [10]. We partition each cell cycle phase into  $N = 20$  stages, giving a total of  $k = 60$  stages for the complete cell cycle. From the start of each phase we set every 10 successive stages to have equal numbers of cells. We therefore only require a total of 6 distinct population parameters.

The vector objective function is  $\mathbf{F}(\mathbf{x}) = [\mathbf{f}_1(\mathbf{x}) \ 10^{-3}\mathbf{f}_2(\mathbf{x}) \ 10^{-3}\mathbf{f}_3(\mathbf{x}) \ 10^{-3}\mathbf{f}_4(\mathbf{x}) \ 10^{-2}\mathbf{f}_5(\mathbf{x})]$ . Trialling different parameters chosen randomly and uniformly from  $(0.1, 1)$  for  $R_i(0)$ ,  $Y_i(0)$  and  $G_i(0)$ , and from  $(4, 20)$  for  $L_r$ ,  $L_y$  and  $L_g$ , we obtain the parameterisation

$$R_i(0) = \begin{cases} 3.47 & \text{for } i = 1, \dots, 10, \\ 2.35 & \text{for } i = 11, \dots, 20, \end{cases} \quad Y_i(0) = \begin{cases} 1.10 & \text{for } i = 1, \dots, 10, \\ 2.09 & \text{for } i = 10, \dots, 20, \end{cases} \quad L_r = 9.22 \text{ h},$$

$$G_i(0) = \begin{cases} 2.68 & \text{for } i = 1, \dots, 10, \\ 1.64 & \text{for } i = 11, \dots, 20, \end{cases} \quad L_y = 5.46 \text{ h}, \quad L_g = 14.44 \text{ h}.$$
(S19)

Note that  $L_r + L_y + L_g = 29.12$  h, in good agreement with the observed cell cycle time of 27 h.

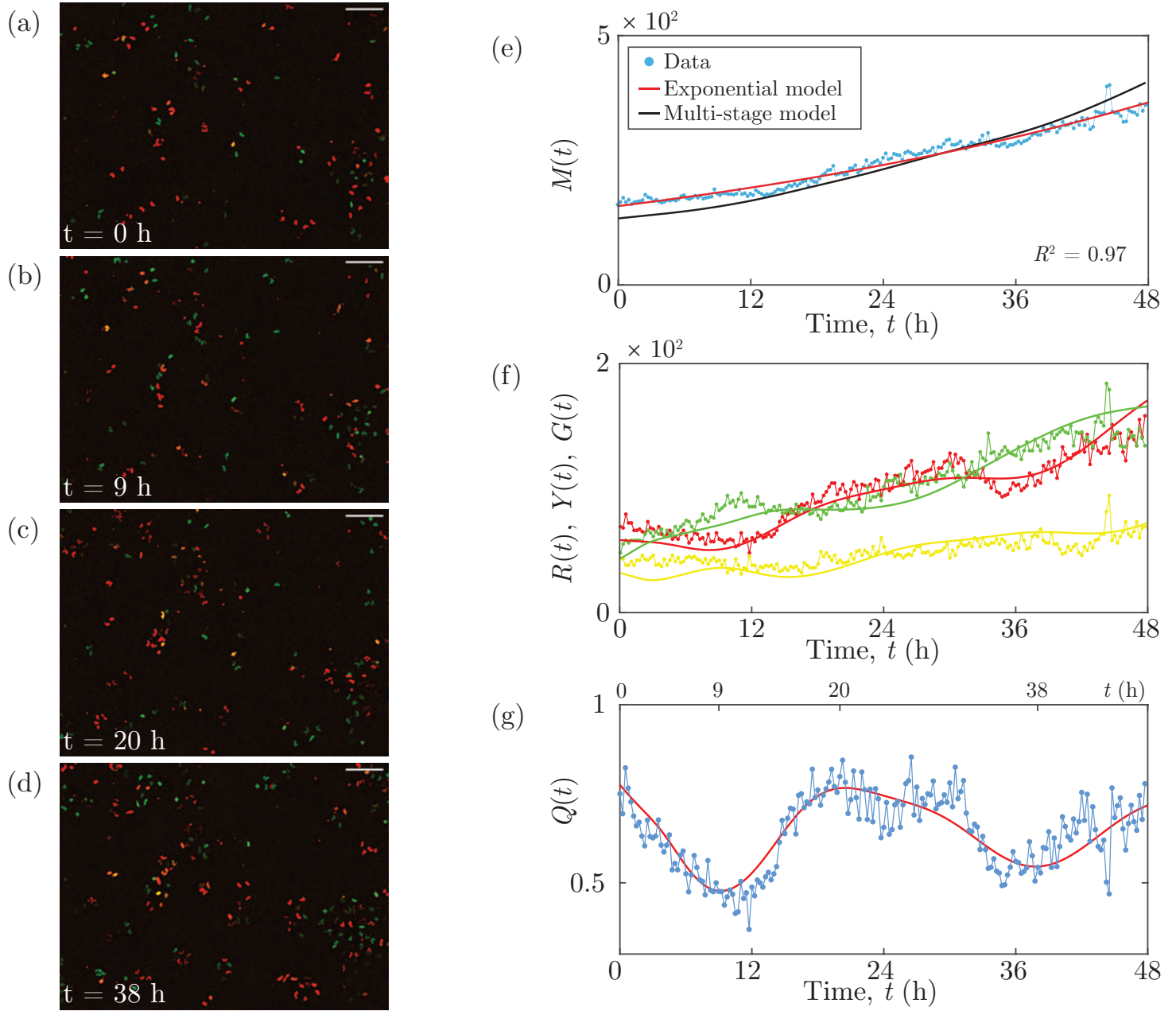


**Figure S6: WM983C experimental data and multi-stage model solution.** (a)–(d) Images of a proliferation assay with FUCCI-WM983C cells. Scale bar 200  $\mu\text{m}$ . (e)  $M(t)$ . Linear regression of  $\ln M(t)$  versus  $t$  provides  $R^2$ . (f)  $R(t)$ ,  $Y(t)$  and  $G(t)$ . (g)  $Q(t)$ . Experimental data are shown as discs and the model solutions as curves.

#### 4.2.8 1205Lu cell line - Figure S7

The experimentally-determined mean cell cycle time for 1205Lu is  $\mathcal{T} = 36$  h [10]. We partition each cell cycle phase into  $N = 20$  stages, giving a total of  $k = 60$  stages for the complete cell cycle. From the start of each phase we set every 5 successive stages to have equal numbers of cells. We therefore only require a total of 12 distinct population parameters.

The vector objective function is  $\mathbf{F}(\mathbf{x}) = [\mathbf{f}_1(\mathbf{x}) \ 10^{-2}\mathbf{f}_2(\mathbf{x}) \ 10^{-2}\mathbf{f}_3(\mathbf{x}) \ 10^{-2}\mathbf{f}_4(\mathbf{x}) \ 0.5\mathbf{f}_6(\mathbf{x})]$ . Starting with the parameters

$$R_i(0) = \begin{cases} 0.27 & \text{for } i = 1, \dots, 5, \\ 0 & \text{for } i = 6, \dots, 10, \\ 21.78 & \text{for } i = 11, \dots, 15, \\ 0 & \text{for } i = 16, \dots, 20, \end{cases} \quad Y_i(0) = \begin{cases} 4.73 & \text{for } i = 1, \dots, 5, \\ 5.39 & \text{for } i = 6, \dots, 10, \\ 0 & \text{for } i = 11, \dots, 15, \\ 2.49 & \text{for } i = 16, \dots, 20, \end{cases} \quad (S20)$$

$$G_i(0) = \begin{cases} 3.15 & \text{for } i = 1, \dots, 5, \\ 5.17 & \text{for } i = 6, \dots, 10, \\ 2.08 & \text{for } i = 11, \dots, 15, \\ 0.45 & \text{for } i = 16, \dots, 20, \end{cases} \quad L_r = 20.97 \text{ h}, \quad L_y = 10.07 \text{ h}, \quad L_g = 10.52 \text{ h},$$

we obtain the parameterisation

$$\begin{aligned}
R_i(0) &= \begin{cases} 0 & \text{for } i = 1, \dots, 5, \\ 13.79 & \text{for } i = 6, \dots, 10, \\ 5.73 & \text{for } i = 11, \dots, 15, \\ 4.19 & \text{for } i = 16, \dots, 20, \end{cases} & Y_i(0) &= \begin{cases} 9.39 & \text{for } i = 1, \dots, 5, \\ 0 & \text{for } i = 6, \dots, 10, \\ 0 & \text{for } i = 11, \dots, 15, \\ 5.04 & \text{for } i = 16, \dots, 20, \end{cases} \\
G_i(0) &= \begin{cases} 2.31 & \text{for } i = 1, \dots, 5, \\ 0 & \text{for } i = 6, \dots, 10, \\ 3.52 & \text{for } i = 11, \dots, 15, \\ 0.63 & \text{for } i = 16, \dots, 20, \end{cases} & L_r &= 19.61 \text{ h}, \\
& & L_y &= 7.99 \text{ h}, \\
& & L_g &= 10.76 \text{ h},
\end{aligned} \tag{S21}$$

Note that  $L_r + L_y + L_g = 38.36$  h, in good agreement with the observed cell cycle time of 36 h.

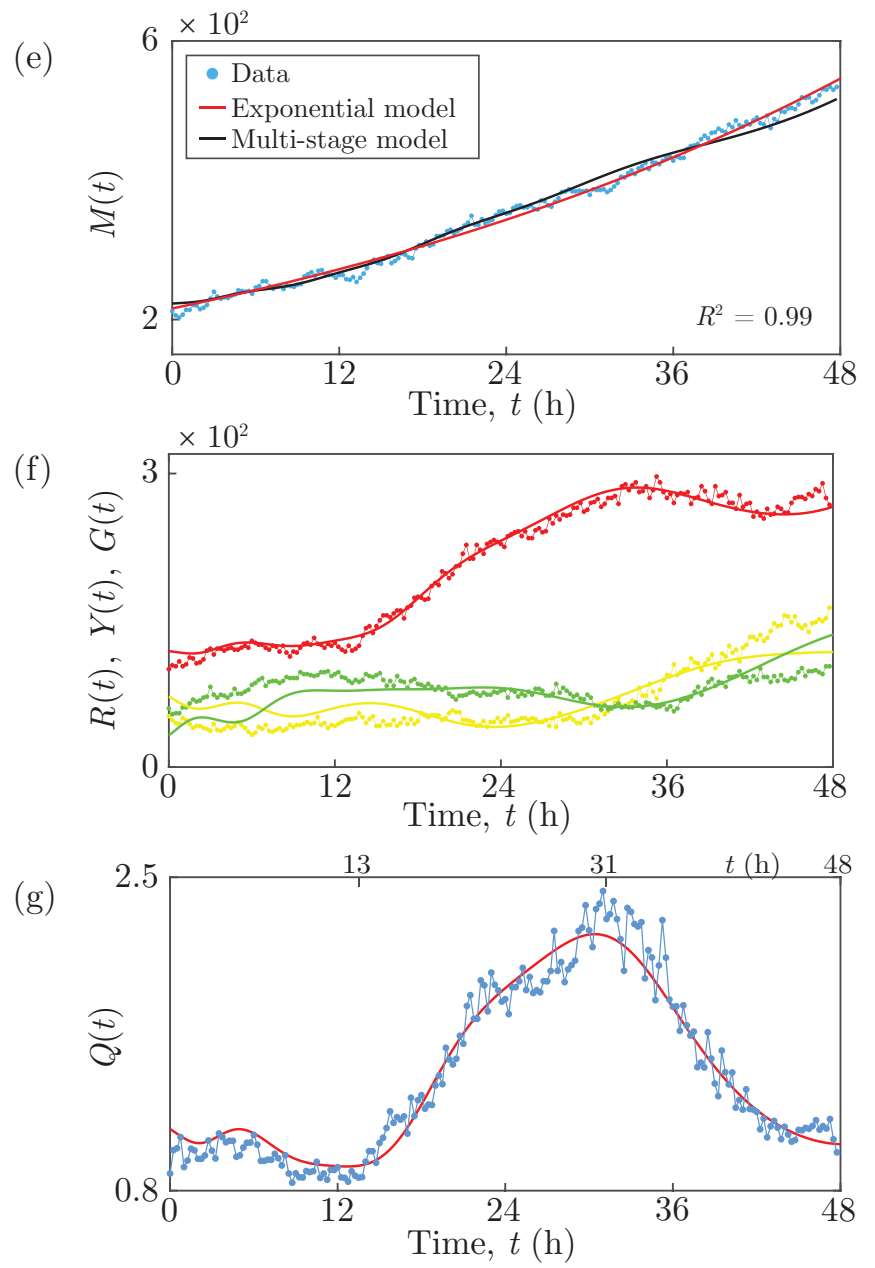
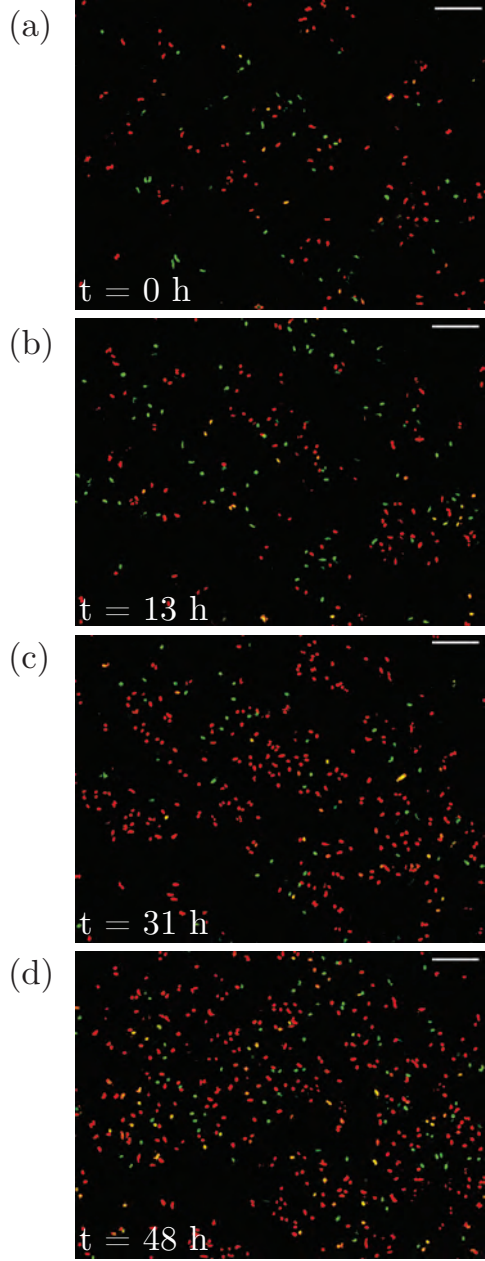


**Figure S7: 1205Lu experimental data and multi-stage model solution.** (a)–(d) Images of a proliferation assay with FUCCI-1205Lu cells. Scale bar 200  $\mu\text{m}$ . (e)  $M(t)$ . Linear regression of  $\ln M(t)$  versus  $t$  provides  $R^2$ . (f)  $R(t)$ ,  $Y(t)$  and  $G(t)$ . (g)  $Q(t)$ . Experimental data are shown as discs and the model solutions as curves.

#### 4.2.9 1205Lu cell line - Figure S8

The experimentally-determined mean cell cycle time for 1205Lu is  $\mathcal{T} = 36$  h [10]. We partition each cell cycle phase into  $N = 20$  stages, giving a total of  $k = 60$  stages for the complete cell cycle. From the start of each phase we set every 4 successive stages to have equal numbers of cells. We therefore only require a total of 15 distinct population parameters.

The vector objective function is  $\mathbf{F}(\mathbf{x}) = [\mathbf{f}_1(\mathbf{x}) \ 10^{-2}\mathbf{f}_2(\mathbf{x}) \ 10^{-2}\mathbf{f}_3(\mathbf{x}) \ 10^{-2}\mathbf{f}_4(\mathbf{x}) \ 0.6\mathbf{f}_6(\mathbf{x})]$ . Trialling different parameters chosen randomly and uniformly from  $(0.1, 1)$  for  $R_i(0)$ ,  $Y_i(0)$  and  $G_i(0)$ , and from  $(4, 20)$  for  $L_r$ ,  $L_y$  and  $L_g$ , we obtain the parameterisation

$$R_i(0) = \begin{cases} 0 & \text{for } i = 1, \dots, 4, \\ 23.75 & \text{for } i = 5, \dots, 8, \\ 0 & \text{for } i = 9, \dots, 12, \\ 13.54 & \text{for } i = 13, \dots, 16, \\ 0.92 & \text{for } i = 17, \dots, 20, \\ 9.94 & \text{for } i = 1, \dots, 4, \\ 0 & \text{for } i = 5, \dots, 8, \end{cases} \quad Y_i(0) = \begin{cases} 12.55 & \text{for } i = 1, \dots, 4, \\ 0 & \text{for } i = 5, \dots, 8, \\ 0 & \text{for } i = 9, \dots, 12, \\ 0 & \text{for } i = 13, \dots, 16, \\ 0.67 & \text{for } i = 17, \dots, 20, \end{cases} \quad (S21)$$

$$G_i(0) = \begin{cases} 3.24 & \text{for } i = 9, \dots, 12, \\ 1.46 & \text{for } i = 13, \dots, 16, \\ 0 & \text{for } i = 17, \dots, 20, \end{cases} \quad L_r = 19.20 \text{ h}, \quad L_y = 7.98 \text{ h}, \quad L_g = 10.89 \text{ h},$$

Note that  $L_r + L_y + L_g = 38.07$  h, in good agreement with the observed cell cycle time of 36 h.

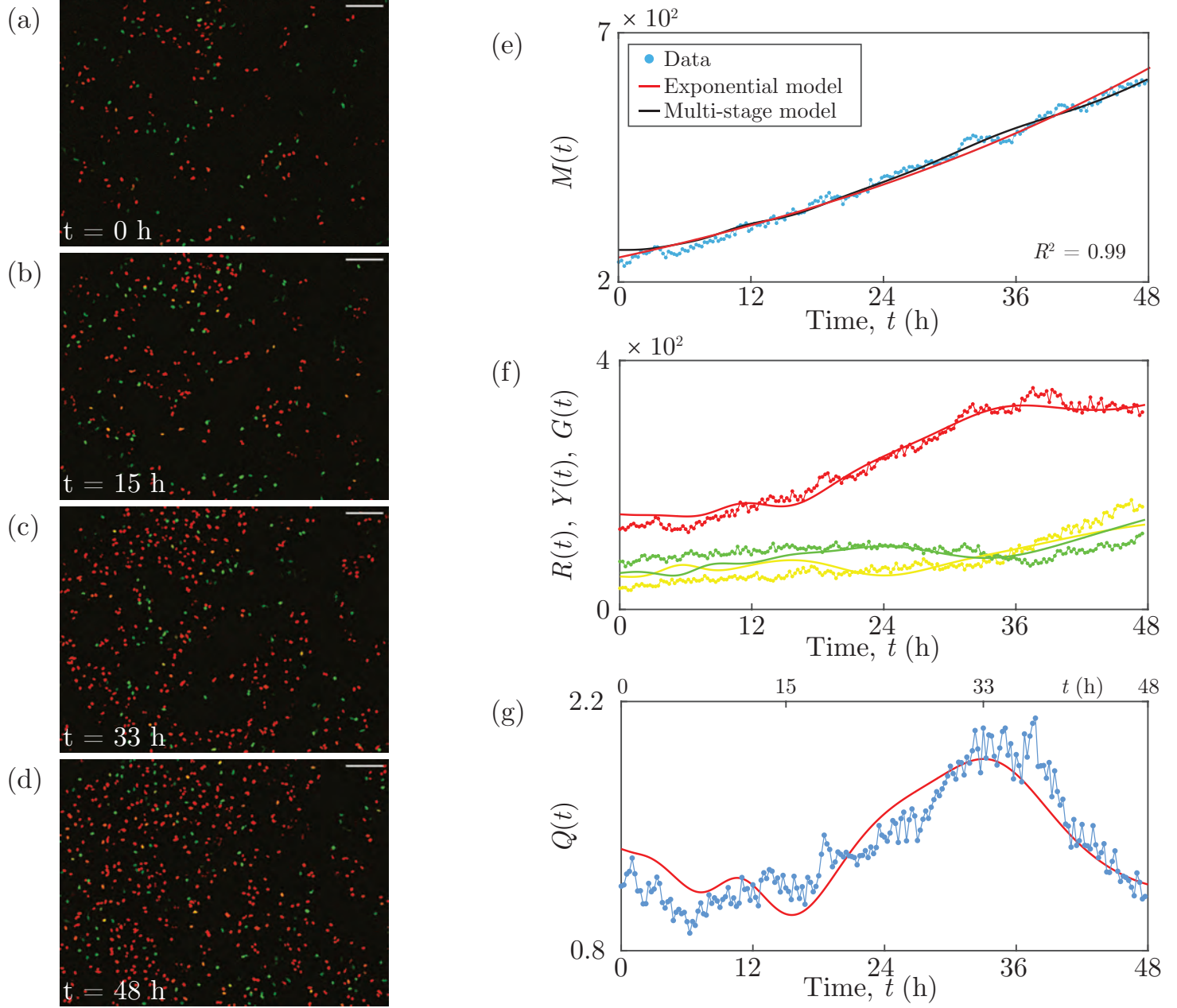


**Figure S8: 1205Lu experimental data and multi-stage model solution.** (a)–(d) Images of a proliferation assay with FUCCI-1205Lu cells. Scale bar 200  $\mu\text{m}$ . (e)  $M(t)$ . Linear regression of  $\ln M(t)$  versus  $t$  provides  $R^2$ . (f)  $R(t)$ ,  $Y(t)$  and  $G(t)$ . (g)  $Q(t)$ . Experimental data are shown as discs and the model solutions as curves.

#### 4.2.10 1205Lu cell line - Figure S9

The experimentally-determined mean cell cycle time for 1205Lu is  $\mathcal{T} = 36$  h [10]. We partition each cell cycle phase into  $N = 12$  stages, giving a total of  $k = 36$  stages for the complete cell cycle. From the start of each phase we set every 3 successive stages to have equal numbers of cells. We therefore only require a total of 12 distinct population parameters.

The vector objective function is  $\mathbf{F}(\mathbf{x}) = [\mathbf{f}_1(\mathbf{x}) \ 3 \times 10^{-3}\mathbf{f}_2(\mathbf{x}) \ 3 \times 10^{-3}\mathbf{f}_3(\mathbf{x}) \ 3 \times 10^{-3}\mathbf{f}_4(\mathbf{x}) \ 0.2\mathbf{f}_6(\mathbf{x})]$ . Trialling different parameters chosen randomly and uniformly from  $(0.1, 1)$  for  $R_i(0)$ ,  $Y_i(0)$  and  $G_i(0)$ , and from  $(4, 20)$  for  $L_r$ ,  $L_y$  and  $L_g$ , we obtain the parameterisation

$$R_i(0) = \begin{cases} 0 & \text{for } i = 1, \dots, 3, \\ 24.89 & \text{for } i = 4, \dots, 6, \\ 25.23 & \text{for } i = 7, \dots, 9, \\ 0 & \text{for } i = 10, \dots, 12, \end{cases} \quad Y_i(0) = \begin{cases} 20.14 & \text{for } i = 1, \dots, 3, \\ 0 & \text{for } i = 4, \dots, 6, \\ 0 & \text{for } i = 7, \dots, 9, \\ 0 & \text{for } i = 10, \dots, 12, \end{cases} \quad (S22)$$

$$G_i(0) = \begin{cases} 2.68 & \text{for } i = 1, \dots, 3, \\ 20.35 & \text{for } i = 4, \dots, 6, \\ 0 & \text{for } i = 7, \dots, 9, \\ 0 & \text{for } i = 10, \dots, 12, \end{cases} \quad L_r = 19.18 \text{ h}, \quad L_y = 9.08 \text{ h}, \quad L_g = 10.99 \text{ h},$$

Note that  $L_r + L_y + L_g = 39.25$  h, in good agreement with the observed cell cycle time of 36 h.

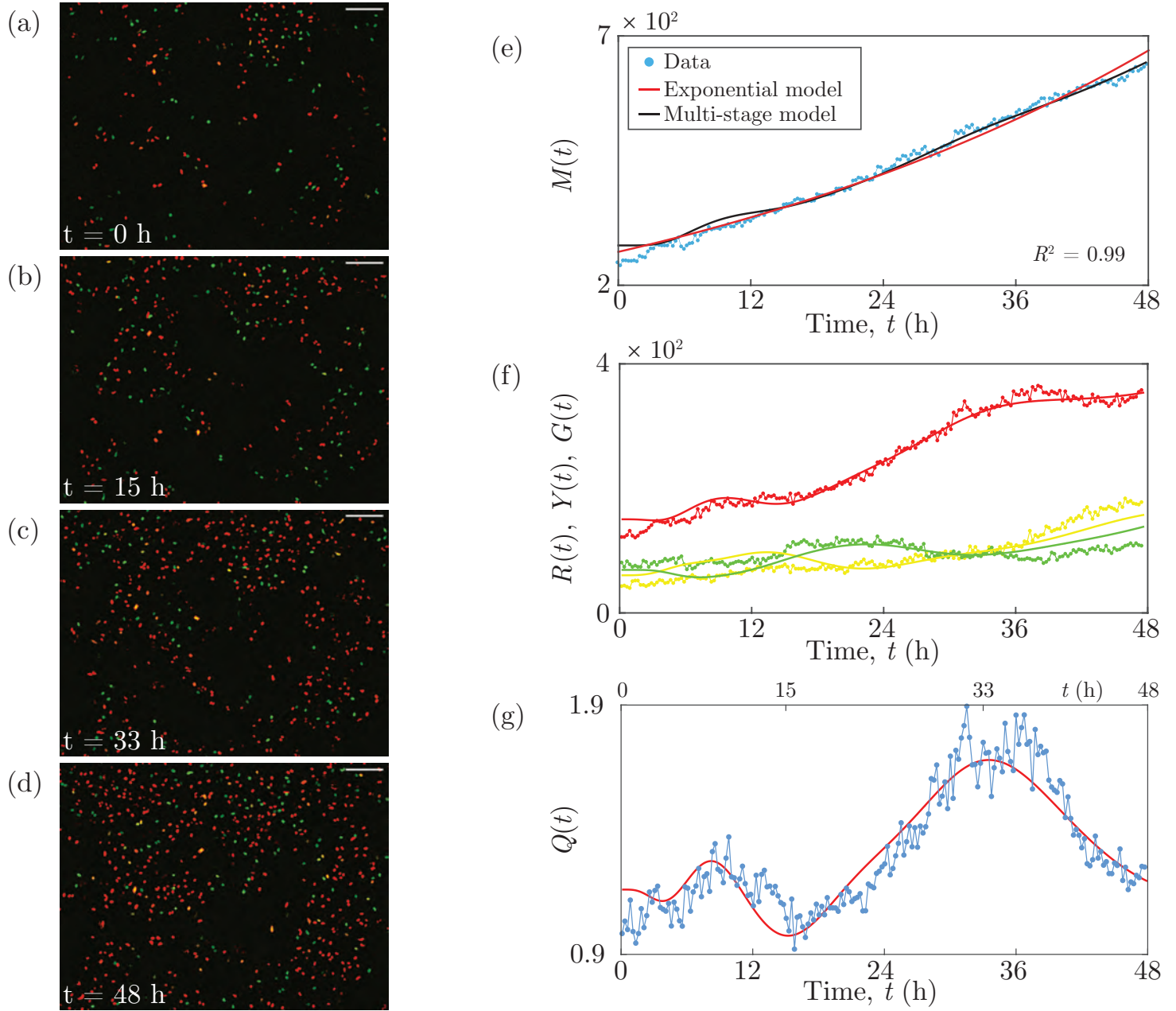


**Figure S9: 1205Lu experimental data and multi-stage model solution.** (a)–(d) Images of a proliferation assay with FUCCI-1205Lu cells. Scale bar 200  $\mu\text{m}$ . (e)  $M(t)$ . Linear regression of  $\ln M(t)$  versus  $t$  provides  $R^2$ . (f)  $R(t)$ ,  $Y(t)$  and  $G(t)$ . (g)  $Q(t)$ . Experimental data are shown as discs and the model solutions as curves.

## 5 All experimental data

Here we provide all of our new experimental data in the following forms:

- The total number of cells  $M(t)$ ;
- The ratio  $Q(t)$  of the number of cells in G1 to the combined number of cells in eS and S/G2/M;
- The discrete Fourier transform of  $Q(t)$ .

These data are obtained from the three cell lines C8161, WM983C and 1205Lu, and four independent experiments. In Experiments 1–3 we use one well of a 24-well plate, and in Experiment 4 we use two wells of a 24-well plate. From each well we obtain time-series stacks at six different positions. These data are available in Supporting Information 2–4, in the form of the number of cells in each phase, G1, eS and S/G2/M, at each time point.

In every experiment, the population growth  $M(t)$  appears to be exponential, and the ratio  $Q(t)$  reveals the presence of inherent synchronisation. In a given well, the six different positions can exhibit different degrees of inherent synchronisation. Further, the synchronisation can be out of phase between the different positions in a given well, and between the different wells.

Note that for some of the data there are a couple of consecutive time points which show a much higher total number of cells than expected, and a corresponding lower ratio in the ratio data. This is due to a large decrease in the signal-to-noise ratio in the green channel at these time points. The specific cause of this is unknown, however fluorescence microscopy is subject to such variations in the signal-to-noise ratio at times. As there is such a large reduction in the signal-to-noise ratio, it is not possible to reduce the unwanted noise without compromising the signal quality.

We provide the discrete Fourier transforms of  $Q(t)$  for every data set to quantitatively demonstrate the existence of oscillating subpopulations in our experimental data. The transforms are obtained using the fast Fourier transform `fft` function [16] in MATLAB, without spectral interpolation. For clarity, we would like the amplitude of the Fourier transform to be zero at zero frequency, so we apply the transform to the time

series  $Q(t) - \overline{Q(t)}$ , where  $\overline{Q(t)}$  is the mean value of the time series. The transformed data are presented as single-sided spectra showing the magnitude of the Fourier transform,  $A(f)$ , as a function of frequency,  $f$ , where  $0 \text{ h}^{-1} \leq f \leq 2 \text{ h}^{-1}$ . Note that the Nyquist frequency is  $2 \text{ h}^{-1}$ .

The Fourier transforms all show dominant frequencies corresponding to periods of either 16, 24 or 48 h, which clearly indicate the presence of oscillations in  $Q(t)$  for each of our data sets, in accordance with the existence of inherent synchronisation. These periods are a reasonable approximation of the experimental cell-cycle durations of the cell lines. To increase the resolution of the frequencies, and thereby obtain better estimates of the periods of the oscillations, a time interval between the time-series images which is less than 15 minutes is required.

## 5.1 C8161 cell line

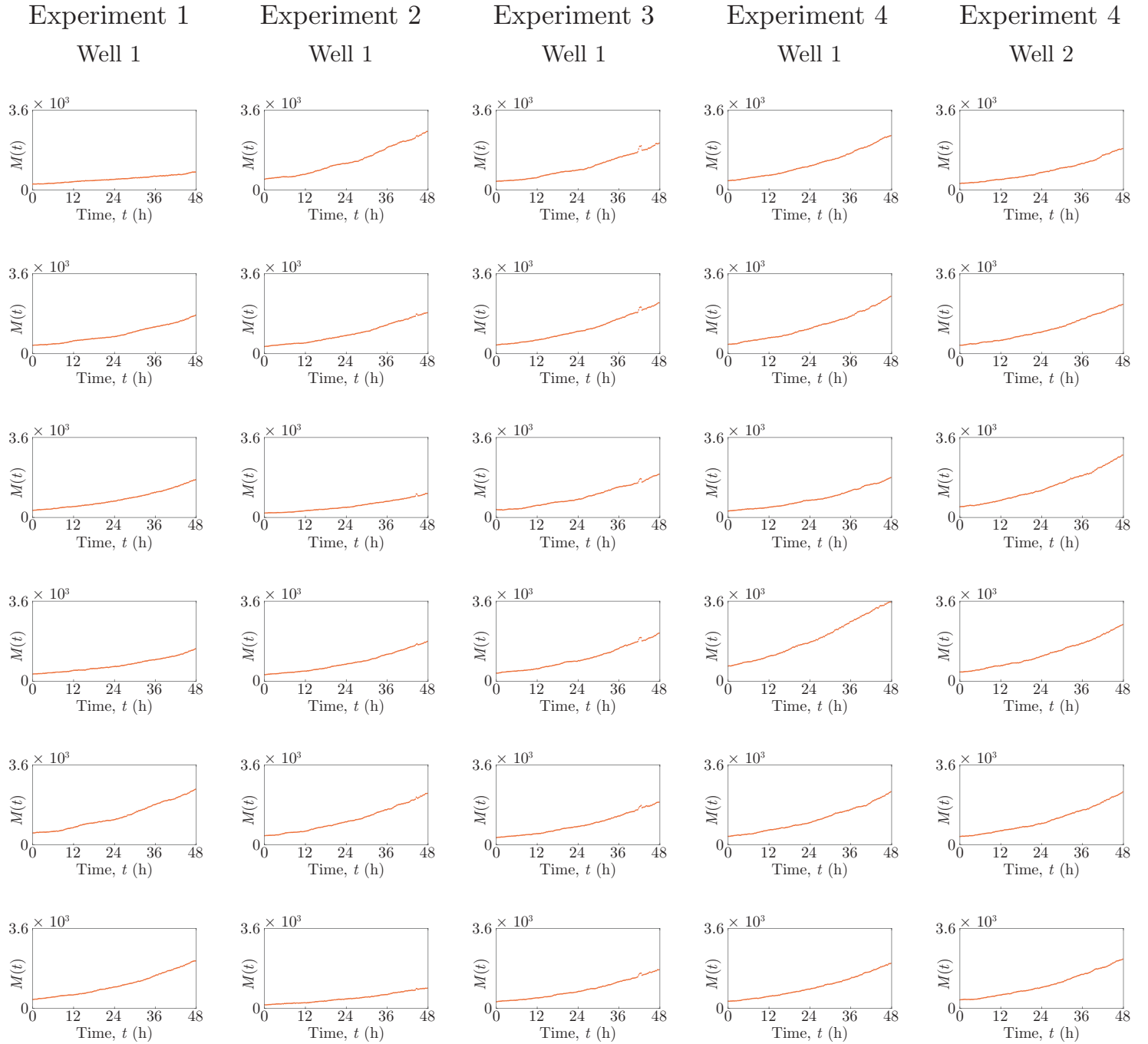


**Figure S10: C8161 experimental data.** Total number of cells  $M(t)$ .

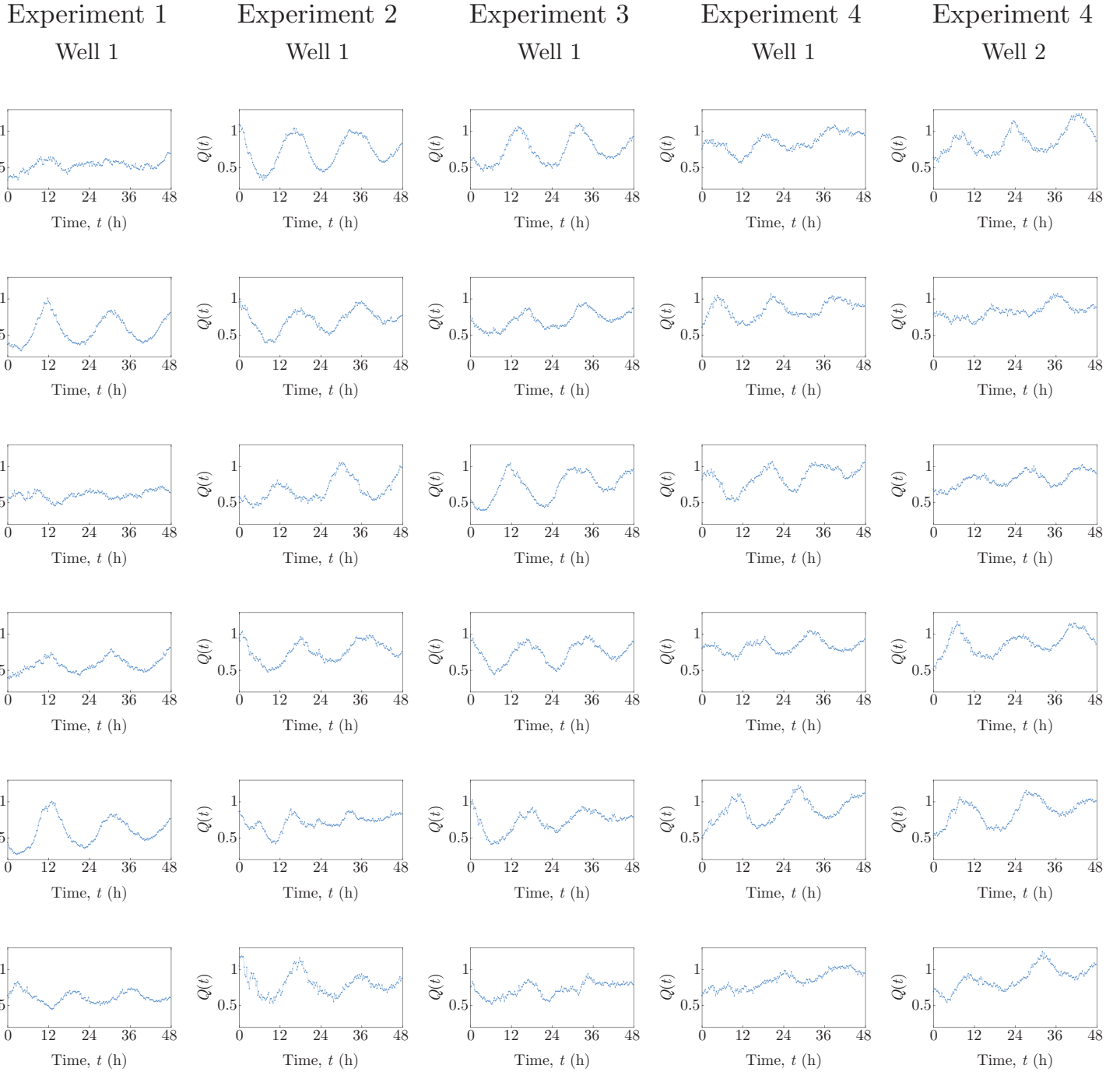


**Figure S11: C8161 experimental data.** Ratio  $Q(t)$  of the number of cells in G1 to the number of cells in eS and S/G2/M.

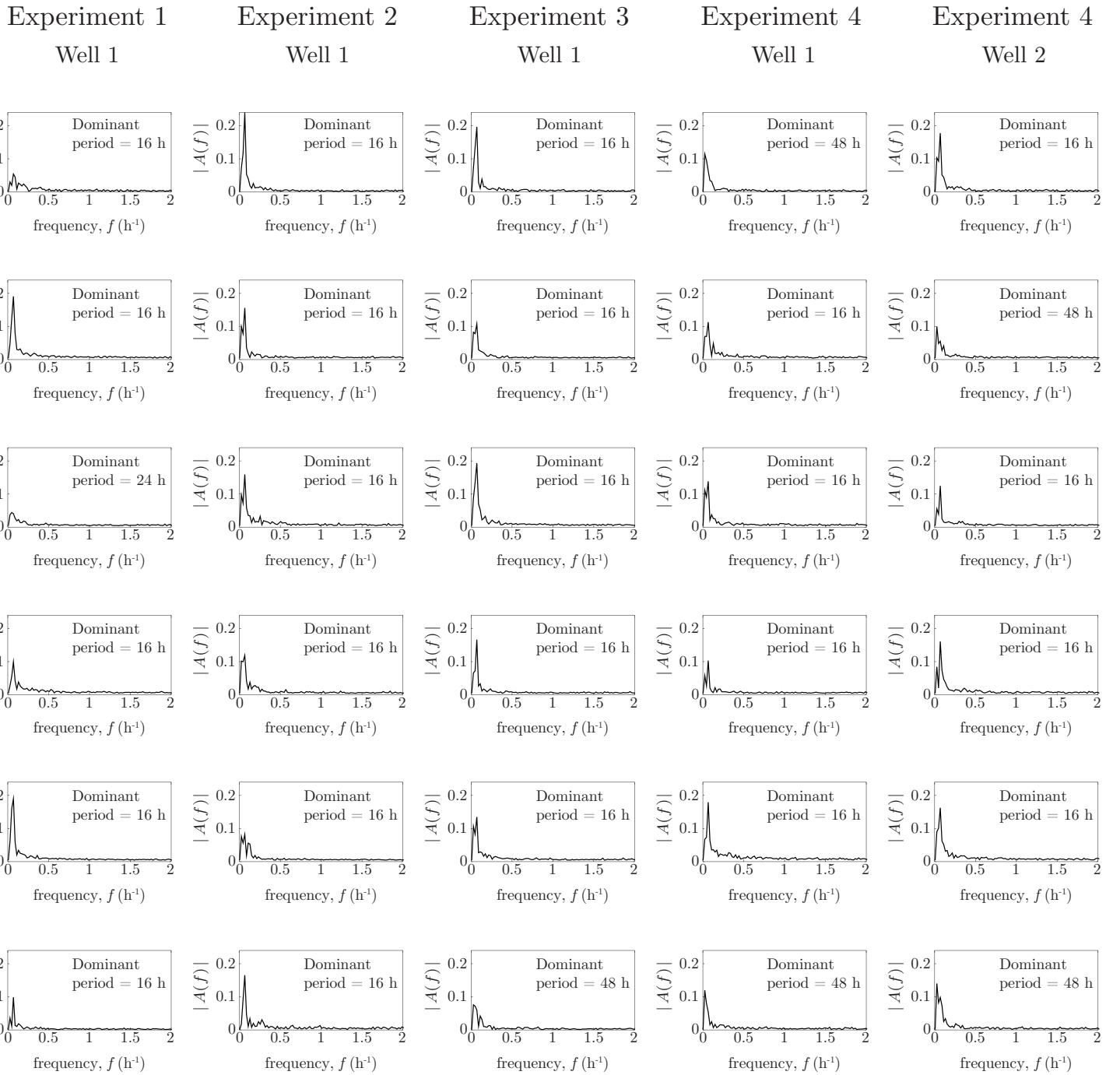


**Figure S12: C8161 experimental data. Magnitude of the Fourier transform,  $A(f)$ , of the ratio  $Q(t) - \overline{Q(t)}$ , as a function of frequency,  $f$ .**

## 5.2 WM983C cell line

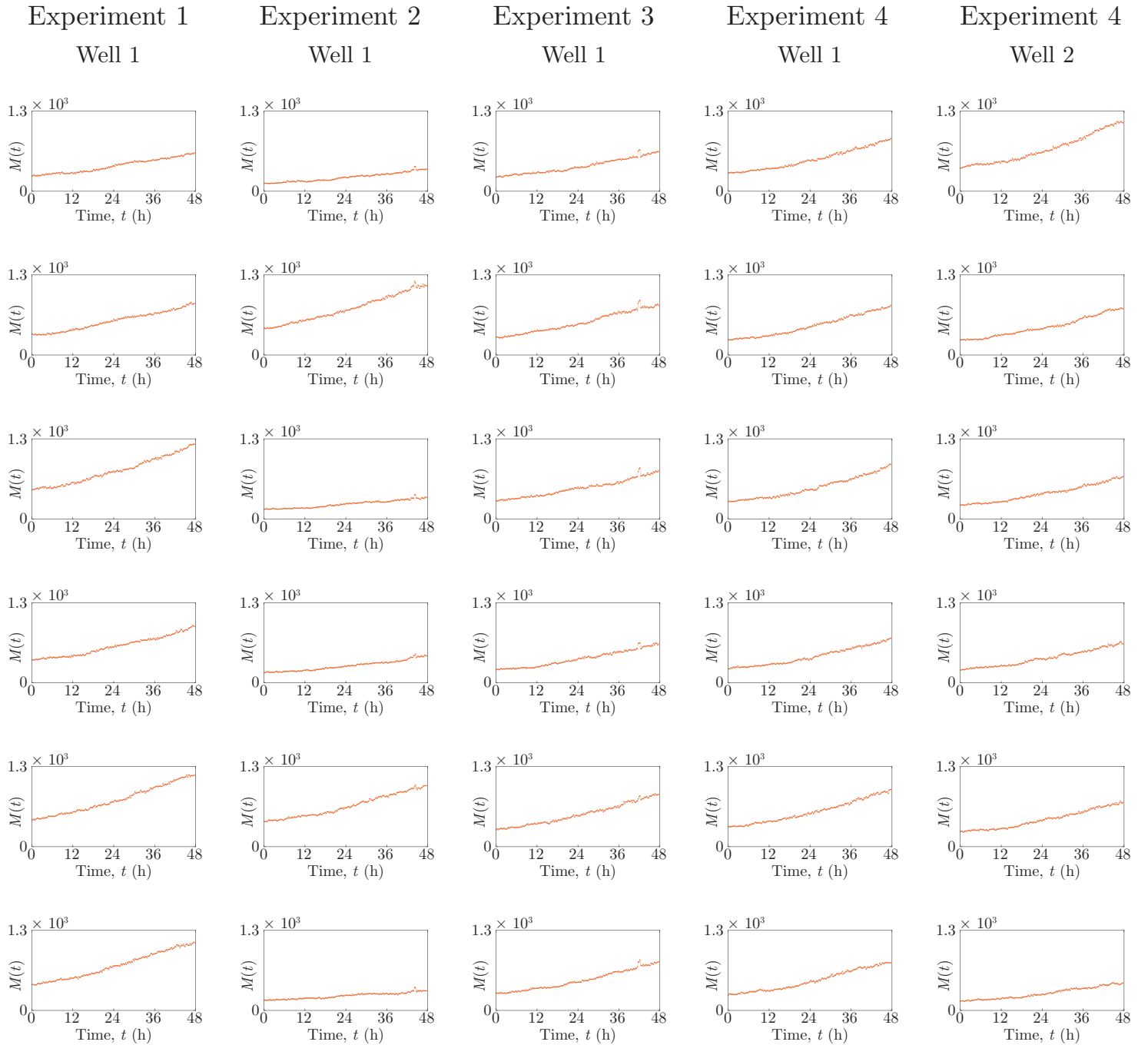


**Figure S13: WM983C experimental data.** Total number of cells  $M(t)$ .

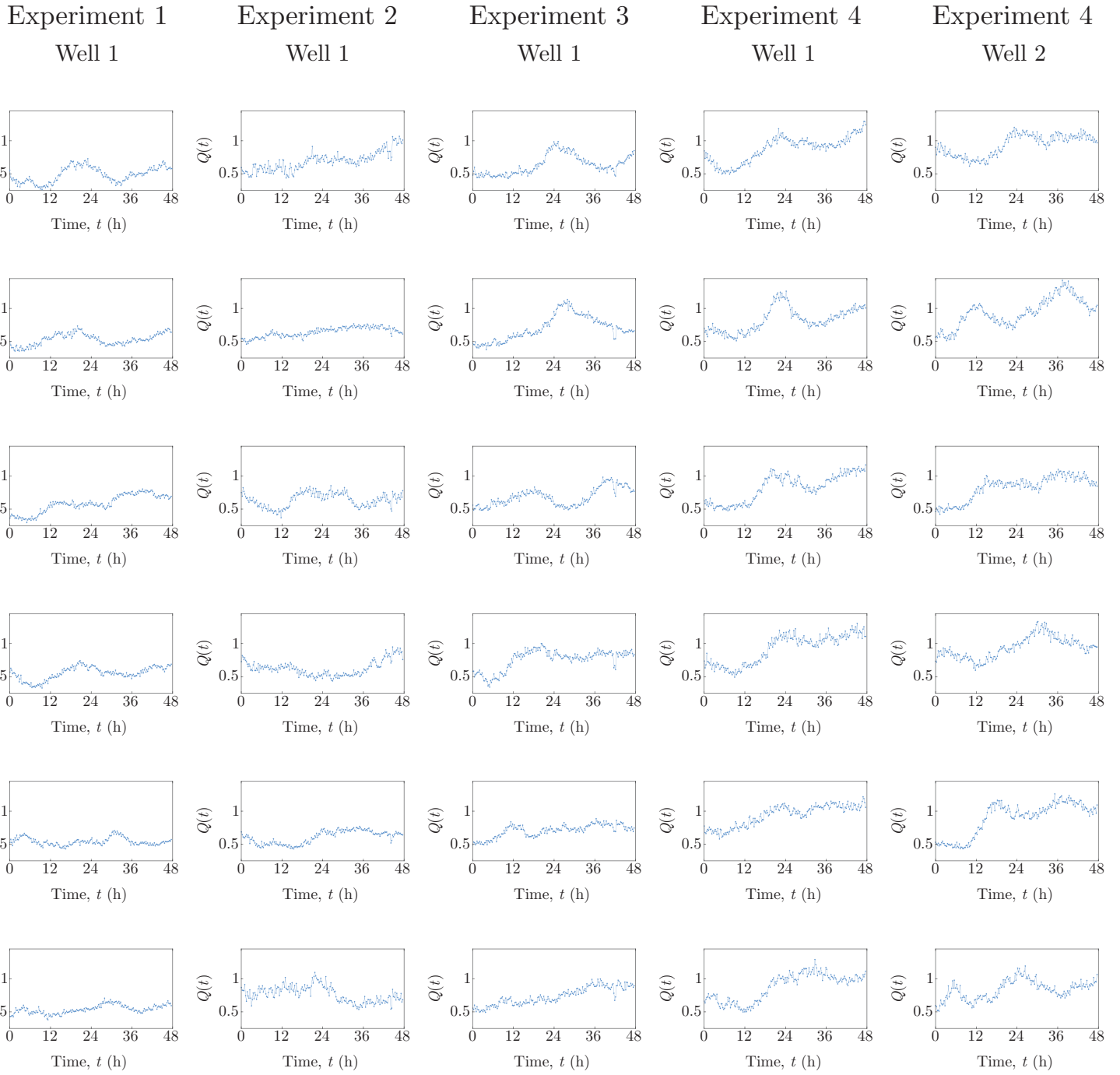


**Figure S14: WM983C experimental data.** Ratio  $Q(t)$  of the number of cells in G1 to the number of cells in eS and S/G2/M.

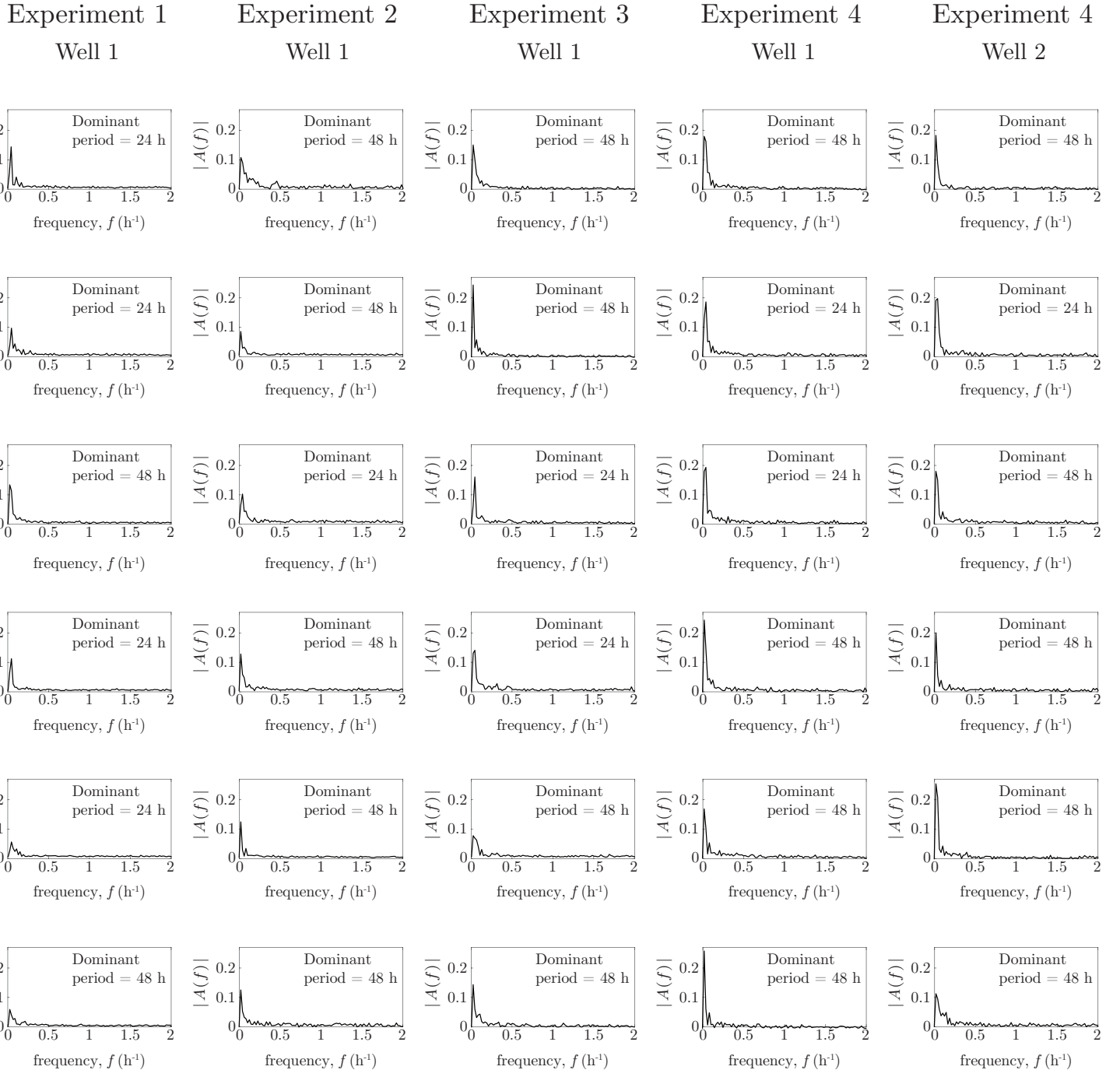


**Figure S15: WM983C experimental data.** Magnitude of the Fourier transform,  $A(f)$ , of the ratio  $Q(t) - \overline{Q(t)}$ , as a function of frequency,  $f$ .

### 5.3 1205Lu cell line

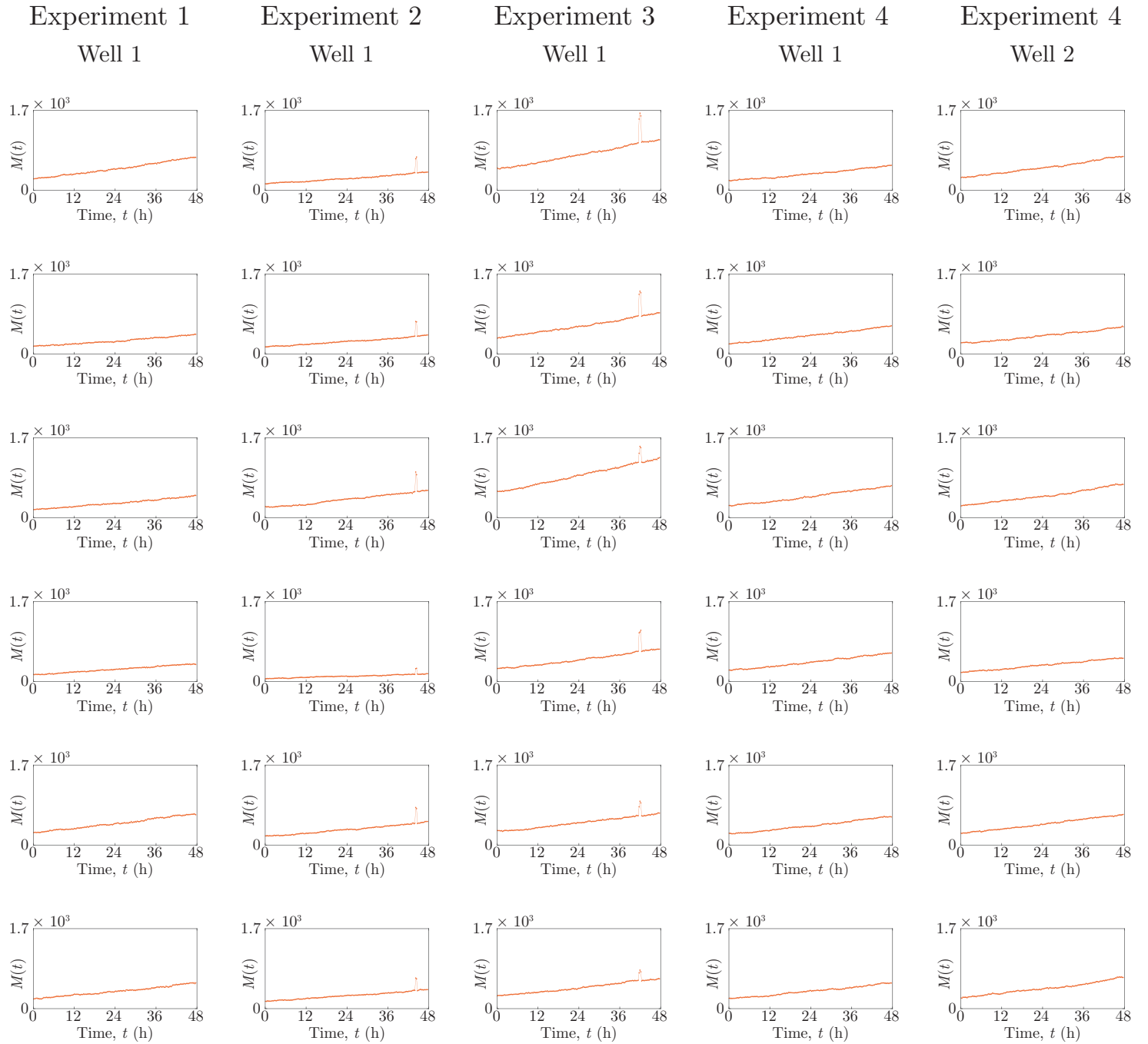


**Figure S16: 1205Lu experimental data.** Total number of cells  $M(t)$ .

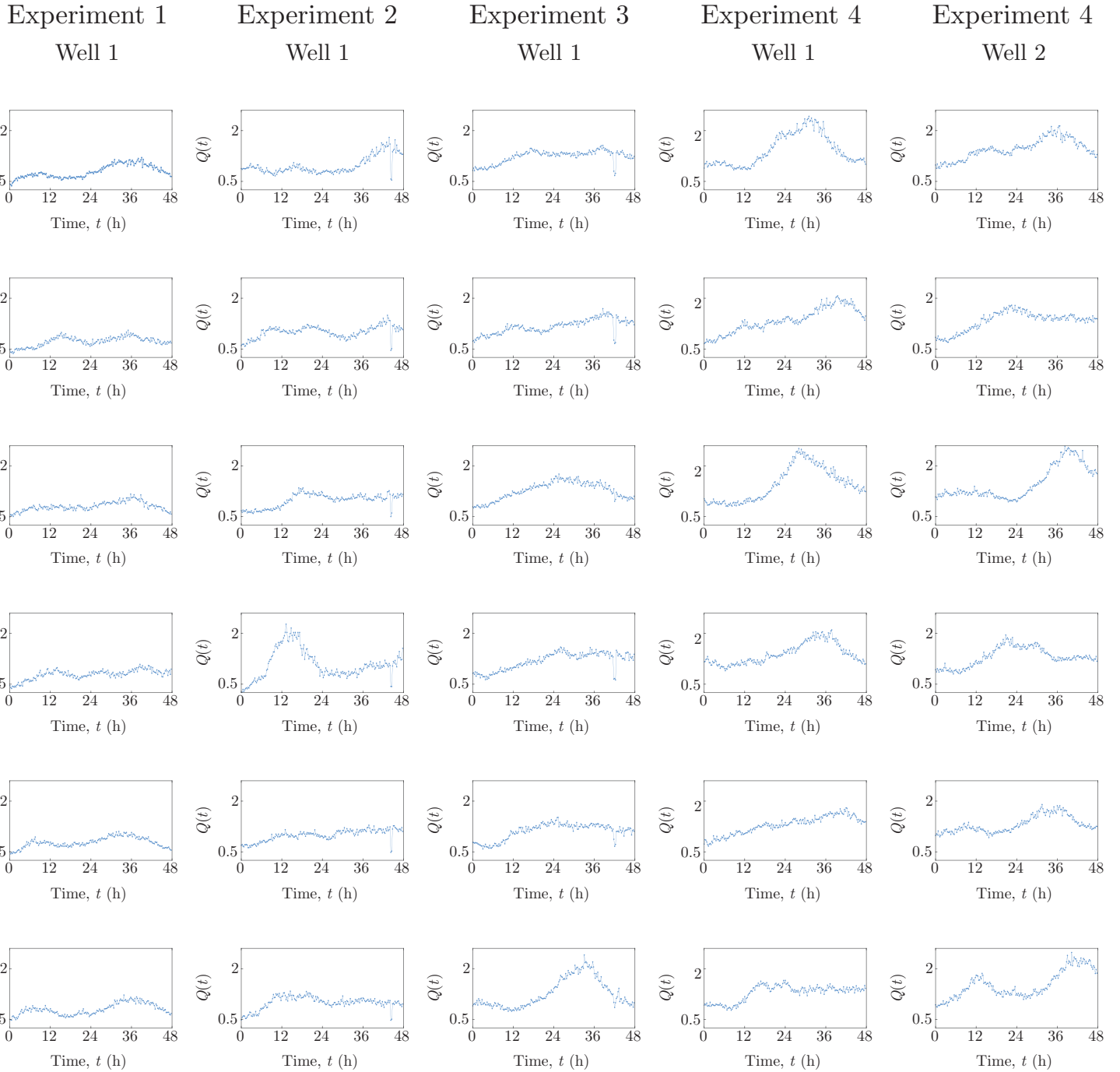


**Figure S17: 1205Lu experimental data.** Ratio  $Q(t)$  of the number of cells in G1 to the number of cells in eS and S/G2/M.

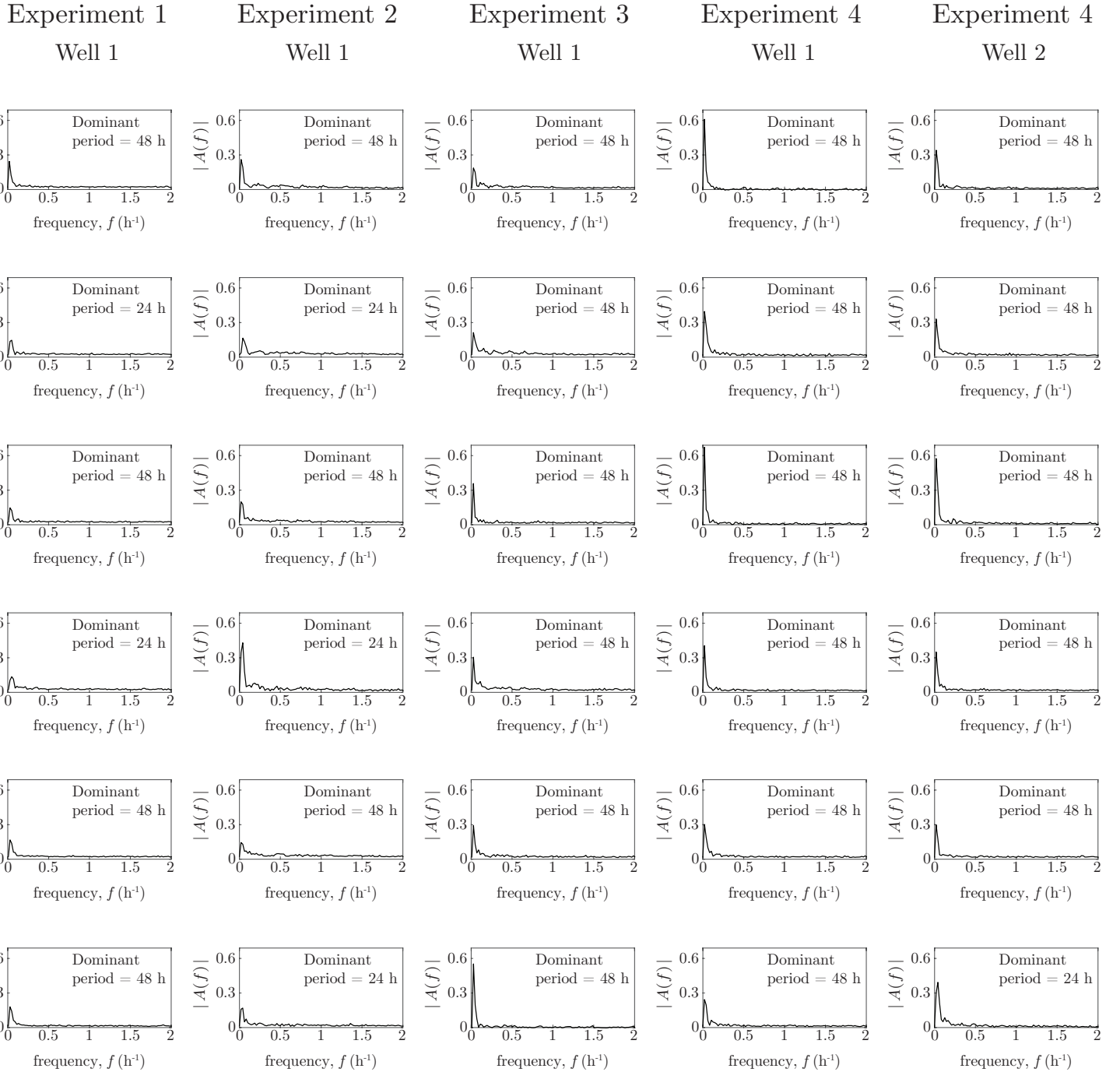


**Figure S18: 1205Lu experimental data.** Magnitude of the Fourier transform,  $A(f)$ , of the ratio  $Q(t) - \bar{Q}(t)$ , as a function of frequency,  $f$ .

## References

- [1] Davies MA, Stemke-Hale K, Lin E, Tellez C, Deng W, Gopal YN, Woodman SE, Calderone TC, Ju Z, Lazar AJ, et al. Integrated molecular and clinical analysis of AKT activation in metastatic melanoma. *Clin Cancer Res.* 2009;15:7538–7546. doi:10.1158/1078-0432.CCR-09-1985.
- [2] Hoek KS, Schlegel NC, Brafford P, Sucker A, Ugurel S, Kumar R, Weber BL, Nathanson KL, Phillips DJ, Herlyn M, et al. Metastatic potential of melanomas defined by specific gene expression profiles with no BRAF signature. *Pigment Cell Res.* 2006;19:290–302. doi:10.1111/j.1600-0749.2006.00322.x.
- [3] Smalley KSM, Contractor R, Haass NK, Kulp AN, Atilla-Gokcumen GE, Williams DS, Bregman H, Flaherty KT, Soengas MS, Meggers E, et al. An organometallic protein kinase inhibitor pharmacologically activates p53 and induces apoptosis in human melanoma cells. *Cancer Research.* 2007;67:209–217. doi:10.1158/0008-5472.CAN-06-1538.
- [4] Smalley KSM, Contractor R, Haass NK, Lee JT, Nathanson KL, Medina CA, Flaherty KT, Herlyn M. Ki67 expression levels are a better marker of reduced melanoma growth following MEK inhibitor treatment than phospho-ERK levels. *Br J Cancer.* 2007;96:445–449. doi:10.1038/sj.bjc.6603596.
- [5] Smalley KSM, Brafford P, Haass NK, Brandner JM, Brown E, Herlyn M. Up-regulated expression of zonula occludens protein-1 in human melanoma associates with N-cadherin and contributes to invasion and adhesion. *Am J Pathol.* 2005;166:1541–1554. doi:10.1016/s0002-9440(10)62370-x.
- [6] Davis PK, Ho A, Dowdy SF. Biological methods for cell-cycle synchronization of mammalian cells. *BioTechniques.* 2001;30:1322–1331. doi:10.2144/01306rv01.
- [7] Taylor IW, Hodson PJ. Cell cycle regulation by environmental pH. *J Cell Physiol.* 1984;121:517–525. doi:10.1002/jcp.1041210310.

- [8] Beaumont KA, Hill DS, Daignault SM, Lui GYL, Sharp DM, Gabrielli B, Weninger W, Haass NK. Cell cycle phase-specific drug resistance as an escape mechanism of melanoma cells. *J Invest Dermatol.* 2016;136:1479–1489. doi:10.1016/j.jid.2016.02.805.
- [9] Sakaue-Sawano A, Kurokawa H, Morimura T, Hanyu A, Hama H, Osawa H, Kashiwagi S, Fukami K, Miyata T, Miyoshi H, et al. Visualizing spatiotemporal dynamics of multicellular cell-cycle progression. *Cell.* 2008;132:487–498. doi:10.1016/j.cell.2007.12.033.
- [10] Haass NK, Beaumont KA, Hill DS, Anfosso A, Mrass P, Munoz MA, Kinjyo I, Weninger W. Real-time cell cycle imaging during melanoma growth, invasion, and drug response. *Pigment Cell Melanoma Res.* 2014;27:764–776. doi:10.1111/pcmr.12274.
- [11] Beaumont KA, Anfosso A, Ahmed F, Weninger W, Haass NK. Imaging- and flow cytometry-based analysis of cell position and the cell cycle in 3D melanoma spheroids. *J Vis Exp.* 2015;106:e53486. doi:10.3791/53486.
- [12] Spoerri L, Beaumont KA, Anfosso A, Haass NK. Real-time cell cycle imaging in a 3D cell culture model of melanoma. *Methods Mol Biol.* 2017;1612:401–416. doi:10.1007/978-1-4939-7021-6\_29.
- [13] The MathWorks, Inc. Fit curve or surface to data; Accessed July 2019. Available from: <https://au.mathworks.com/help/curvefit/fit.html>.
- [14] The MathWorks, Inc. Solve nonlinear least-squares (nonlinear data-fitting) problems; Accessed July 2019. Available from: <https://mathworks.com/help/optim/ug/lsqnonlin.html>.
- [15] Coleman TF, Li Y. An interior trust region approach for nonlinear minimization subject to bounds. *SIAM J Optim.* 1996;6:418–445. doi:10.1137/0806023.
- [16] The MathWorks, Inc. Fast Fourier transform; Accessed July 2019. Available from: <https://au.mathworks.com/help/matlab/ref/fft.html>.